LUND UNIVERSITY

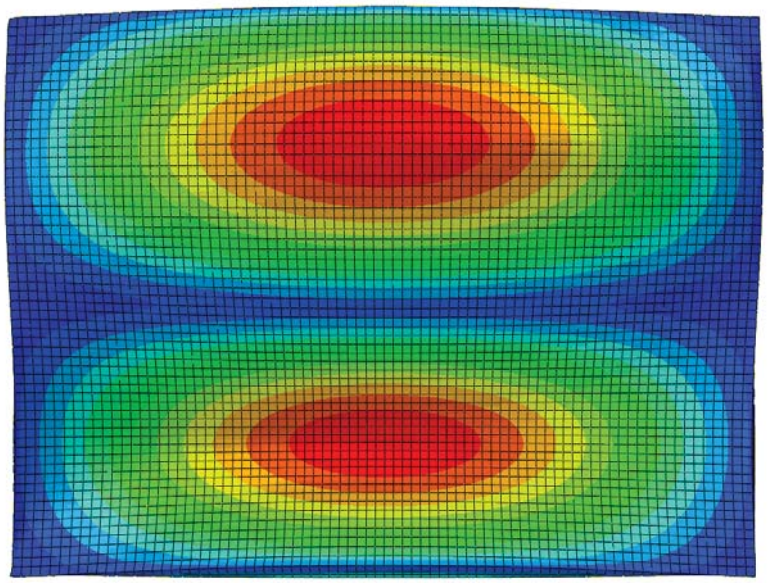

FEM MODELLING OF SOUND REDUCTION INDEX IN PARTITION CLT WALL

ERIK HÖRSTRÖM and ADAM HULTIN

Engineering Acoustics

Master's Dissertation

DEPARTMENT OF CONSTRUCTION SCIENCES

DIVISION OF ENGINEERING ACOUSTICS

ISRN LUTVDG/TVBA--20/5058--SE (1-66) | ISSN 0281-8477

MASTER'S DISSERTATION

FEM MODELLING OF SOUND REDUCTION INDEX IN PARTITION CLT WALL

ERIK HÖRSTRÖM and ADAM HULTIN

Supervisor: **DELPHINE BARD**, Associate Professor, Div. of Engineering Acoustics, LTH, Lund.

Examiner: Professor **KENT PERSSON**, Div. of Structural Mechanics, LTH.

Printed by V-husets tryckeri LTH, Lund, Sweden, January 2020 *(Pl)*.

For information, address:
Division of Engineering Acoustics,
Faculty of Engineering LTH, Lund University, Box 118, SE-221 00 Lund, Sweden.
Homepage: www.akustik.lth.se

Abstract

Constructing buildings with wood brings many advantages, especially regarding environmental aspects, which has brought an up-rise in these types of structures. However, one of the main issues regarding wooden structures is its tendency to perform poorly acoustically in lower frequencies compared to heavier structures. This often leads to unwanted noise levels which could be avoided in earlier design stages with tools that predicts the vibroacoustic response. Predicting the vibroacoustic response of buildings constructed with wood is challenging much due to its irregular material parameters. Wood is an orthotropic material meaning it has varying stiffness and strength in different directions. It is also an organic material which brings a variation in stiffness and strength not only between different species of trees, but also within the same species. In order to have building elements with less variation regarding these parameters, different engineered wood products (EWPs) has emerged on the market during the last decades. Cross-laminated timber (CLT) is an increasingly popular product in the wooden building industry which demands for more research of its vibroacoustic performance.

In this thesis a finite element model was created to predict the airborne sound insulation of a five-layer CLT slab in the low-frequency range of 1-200 Hz. Different measurements, such as experimental modal analysis and sound pressure level measurements, were performed to calibrate the model as well as validate the results obtained from it. The thesis shows that the airborne sound insulation can be predicted with a finite element model, but only together with measurements determining the material parameters and damping of the CLT under evaluation. The damping was shown to have a crucial impact on the results. The airborne sound insulation is determined in the model at the excited resonance frequencies of a plate due to a pressure load resembling airborne sound.

Acknowledgments

This thesis was written during the spring of 2019 for the division of Engineering Acoustics at Lund University. We would like to thank our deputy supervisor Cheng Qian for all the guidance and endless running between her office and the lab facility to unlock the door for us. We would also like to thank our supervisor Delphine Bard and examiner Kent Persson for all the help.

Erik Hörström & Adam Hultin

Lund, 2019

Table of content

1 Introduction

1.1 Background

Densification of cities due to growing population in towns brought alongside high-rise buildings, which are more often being constructed with timber. Today, 10 % of Sweden's multi-dwelling buildings are built with wood and in 2025 the proportion is expected to have increased to 50 % [1]. This increase of timber structures is due to the many advantages of building with wood. First and foremost, wood is a light material allowing construction on weaker foundations. There is even the possibility to build on already existing foundations without reinforcing it. An example of this is the project Kv Kullen in Rundvik, Sweden, where a multi-story wooden residential building was constructed on an already existing car park. Building with timber also allows a high degree of prefabrication, in the form of building elements such as walls and floors, or even full-scale room volumes. The lightness of timber contributes to the prefabrication aspect, since it allows large quantities to be transported efficiently. Building with prefabricated elements has been shown to reduce the construction time with 20 % to 70 %, with a reduced waste at the construction sites [4].

Timber is an organic and renewable building product, making it a sustainable alternative to other common building materials. The carbon footprint is greatly reduced when wood is used as the main structural material compared to other options, such as steel or concrete. A study made by KTH and IVL [2] comparing the emissions of constructing multi-story buildings with wood instead of concrete showed that the climate influence was halved. From a Swedish perspective, a land covered in 70% forest and where the timber biomass has been increasing ever since the beginning of the 20th century [5], wood as a building material has a huge potential.

Wood, being a biological material, exhibit variations in material parameters. In order to enhance the structural properties of timber, so called engineered wood products (EWPs) has been introduced over the years. Examples of this type of products are OSB, glulam, and the focus point of this thesis: Cross-Laminated Timber (CLT). CLT is a massive wood construction product in the form of plates made up of at least three layers of panels that are bonded together crosswise. These plates serve both the purpose of room separation and load bearing, making it an efficient building element. CLT can be used as walls, floors and roofs. In practice, whole buildings can be constructed entirely with CLT. With the predicted increase of wooden buildings CLT is expected to play a big role, with some of the largest forest industry concerns in Sweden making big investments in the product [28].

The main drawback with wooden constructions is however the acoustic performance at the lower frequencies. Wood behaves rather well when it comes to sound insulation at high frequencies where it is comparable or even outperform heavier building materials such as concrete. When comparing in the low-frequency range, concrete structures displays up to 20 dB better airborne sound insulation than wooden structures [3]. Existing vibration sources such as motorways, railways, harbors or simply the neighbors' daily activities can have a very high impact on the vibroacoustic behavior of such structures, triggering complaints from the people living in them.

Noise exposure is, according to the World Health Organization (WHO), among the top environmental risks to physical- and mental health [6] where approximately two million people in Sweden are exposed to a noise level that exceeds current regulations. Acoustic insulation of buildings is therefore an important concern during the design- and construction phase. There

are regulations, such as International Organization of Standardization (ISO), with requirements that needs to be fulfilled in order to achieve good acoustic comfort.

The acoustical performance of timber structures is hard to predict since it is highly dependent on the construction method and varies substantially with different types of building elements. Current ISO evaluation methods and regulations regarding acoustics are based on heavier constructions, often resulting in wrong predictions of lighter ones. The consequences of failed projecting are much more severe for lightweight structures compared to heavier ones. These uncertainties cause hesitation among developers, that tend to choose the more predictable heavier constructions [3]. Therefore, better prediction tools are sought after. Today, software such as Abaqus using the finite element method (FEM) is widely available and is a strong tool for predicting low frequency response.

1.2 Aim and objective

The aim of this thesis is to investigate the crucial parameters involved when making a FE model of CLT such as boundary conditions, damping and material parameters using the commercial software Abaqus in order to capture the vibroacoustic response in the low-frequency range (1-200Hz). The response will then be used to predict the airborne sound insulation of CLT. The FE model is validated by the results from laboratory measurements of a five-layer CLT slab. The measurements are conducted in the laboratory facilities of LTH in accordance with the current ISO standards.

1.3 Limitations

One of the limitations of this thesis is to strictly treat vibroacoustic response for lower frequencies, defined in a band between 1-200 Hz. The effect of the adhesives bonding the CLT is considered negligible and not accounted for. Flanking transmission is also out of the scope of this thesis.

1.4 Method

The method to reach the goal of the thesis, determining the airborne sound insulation through a numerical model, is to by different measurements construct and validate a FE model in the software Abaqus. Firstly, a theoretical study was made regarding the fundamental theory revolving around the problem at hand. This includes the material characteristics of wood, the theory of acoustics and structural dynamics and the finite element method. Secondly, measurements were conducted for different purposes:

- An experimental modal analysis was performed to determine the material parameters of the CLT, in a lab setup where the boundary conditions were somewhat controlled. The results were used to calibrate the FE model.
- Sound reduction measurements were conducted with the CLT placed in a sound transmission lab. The results were used to later compare with the sound reduction obtained from the model.
- Damping measurements were performed in the transmission lab in order to determine the damping in this specific setting.

The results from the different measurements were then used to finalize an Abaqus FE model which output can be used to predict the airborne sound insulation.

1.5 Outline

Chapter 1 contains information about the background, aim, method and limitations of the thesis.

Chapter 2 explains the characteristics of wood as a building material, clarifying its orthotropic nature and deriving its material parameters. It also contains an introduction to the wooden product CLT.

Chapter 3 introduces the basic acoustic theory including sound pressure level, waves, sound transmission, sound insulation, reverberation time and sound radiated from a vibrating plate.

Chapter 4 explains the basic theory of structural dynamics, applicable in acoustic problems.

Chapter 5 briefly introduces the FEM, explaining the essentials of the method such as element types, mesh and modes as well as methods to validate a FE model by measurements.

Chapter 6 contains the results of a material parameter study, obtained by calibrating an Abaqus model with measurement results from an experimental modal analysis.

Chapter 7 displays the results of sound measurements conducted in a transmission lab, culminating in determination of the sound reduction index. It also details the final Abaqus model that is used to predict the airborne sound insulation.

Chapter 8 discusses the results obtained and how it can be used and brings uncertainties to light.

Chapter 9 presents the conclusions of the thesis.

2 Wood

Wood is a biological material with a complex mechanical behavior. Like most other organic materials, the mechanical response is directly connected to the way the plant grows. Wood mainly consist of (90-95%) long, hollow cells, commonly referred to as fibers. During a tree's life these fibers transports water through the plant, comparable with the vascular system transporting blood through the human body. The tree grows in height but also in thickness in a circular expansion from its center. During the spring and early summer, the tree grows quick and light earlywood is formed. During the summer the growth is slower and darker latewood is formed. This phenomenon can easily be observed as growth rings in the cross-section of a log. The growth rings and the fiber direction dominate the anatomy of wood and dictates its properties [9].

2.1 Material properties

With the fibers growing in the tree's length direction together with the radial growth in its thickness makes wood an orthogonal anisotropic material, commonly known as orthotropic, meaning it has three symmetry planes with different material properties in the three main directions. A Cartesian coordinate system is adopted to distinguish orientation (figure 1) with one axis along the fiber direction (L), one radially to the growth rings (R) and one tangentially to the growth rings (T).

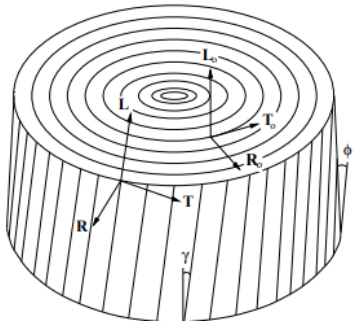

Figure 1. Cartesian coordinate system on the cross-section of a log. (Persson, 2000)

The strength and stiffness of wood in its strongest material direction, along its fibers (L), is very high in relation to its material weight. However, in the other two directions (R, T) wood is relatively weak and soft where the stiffness in the radial direction is about 1.5 times higher than in the tangential direction. In addition, the strength of wood varies with temperature and moisture content and due to natural variations in the wood, such as residue pockets and knots. This discrepancy is present not only in different trees, but also within the same tree [7]. The variation causes the material to be prone to cracking under loading and entails thoughtful orientation when used as a building material.

Wood, like many organic materials, is very complex to describe in terms of material parameters. Variations occur on a microscopic level during its growth due to factors such as wind, precipitation and soil [7]. However, on the macro-scale suitable for acoustic modelling, assuming linear elastic behavior, wood can be described with three material parameters in each of the three main directions. These are the elastic modulus E_L, E_R, E_T, the shear modulus G_{LR}, G_{LT}, G_{RT} and the Poisson's ratio $\nu_{RL}, \nu_{LT}, \nu_{RT}$ [8]. The constitutive behavior of wood can be described by Hooke's generalized law with these parameters by use of matrix notation as:

$$\boldsymbol{\epsilon} = \boldsymbol{C\sigma} \tag{2.1}$$

Or in full display:

$$\begin{bmatrix} \epsilon_{LL} \\ \epsilon_{RR} \\ \epsilon_{TT} \\ \gamma_{LR} \\ \gamma_{LT} \\ \gamma_{RT} \end{bmatrix} = \begin{bmatrix} \frac{1}{E_L} & -\frac{\nu_{RL}}{E_R} & -\frac{\nu_{TL}}{E_T} & 0 & 0 & 0 \\ -\frac{\nu_{LR}}{E_L} & \frac{1}{E_R} & -\frac{\nu_{TR}}{E_T} & 0 & 0 & 0 \\ -\frac{\nu_{LT}}{E_L} & -\frac{\nu_{RT}}{E_R} & \frac{1}{E_T} & 0 & 0 & 0 \\ 0 & 0 & 0 & \frac{1}{G_{LR}} & 0 & 0 \\ 0 & 0 & 0 & 0 & \frac{1}{G_{LT}} & 0 \\ 0 & 0 & 0 & 0 & 0 & \frac{1}{G_{RT}} \end{bmatrix} \begin{bmatrix} \sigma_{LL} \\ \sigma_{RR} \\ \sigma_{TT} \\ \tau_{LR} \\ \tau_{LT} \\ \tau_{RT} \end{bmatrix} \tag{2.2}$$

The inverse relation is perhaps more commonly used:

$$\boldsymbol{\sigma} = \boldsymbol{D}\boldsymbol{\epsilon} \tag{2.3}$$

Where $\boldsymbol{\epsilon}$ is the elastic strain vector, $\boldsymbol{\sigma}$ the stress vector and $\boldsymbol{D}$ the material stiffness matrix which is the inverse of $\boldsymbol{C}$. Note that due to the linear elastic assumption, the material stiffness matrix $\boldsymbol{D}$ is symmetric. This results in:

$$\frac{\nu_{RL}}{E_R} = \frac{\nu_{LR}}{E_L}; \quad \frac{\nu_{TL}}{E_T} = \frac{\nu_{LT}}{E_L}; \quad \frac{\nu_{TR}}{E_T} = \frac{\nu_{RT}}{E_R} \tag{2.4}$$

Giving the previously stated 9 independent parameters describing the material stiffness. The CLT is modeled in this manner in the FE analyses carried out in this thesis.

The large variation in material parameters found in different wood samples makes it hard to model correctly. In fact, a correct model is not likely to be obtained by choosing material parameters from a general table. The parameters must be customized for the specific building element tested. This can be achieved by fitting a model to experimental results.

2.2 CLT

In order to enhance the structural properties of timber building materials, so called engineered wood products has been introduced over the years. Most of these products consist of smaller pieces of wood, e.g. splinters and veneers, bonded together with glue or by heat and pressure, and then formed into building elements such as panels. By doing so, some of the negative effects due to irregularities of wood, such as resin pockets, and knots are reduced. It also brings the possibility to create building elements of any wanted size with customized properties [9]. Examples of this type of products are Oriented Strand Boards (OSB), glulam, and Cross-Laminated Timber (CLT). CLT is a massive wood construction product made of at least three layers of panels that are bonded together crosswise with adhesives. The panels consist of glued boards or planks. Each layer of panel is rotated in 90 degrees in relation to the neighboring layer. By assembling in this perpendicular fashion, the large difference between longitudinal and horizontal stiffness found in a single wooden plank is reduced. The two outer layers are always oriented in the load-bearing direction, and since CLT are produced in an odd number of layers, normally 3, 5 or 7, the plate will always be stiffer in one direction. The layers can be of varying thickness and timber quality dependent on the manufacturer, due to the current lack of regulations [21].

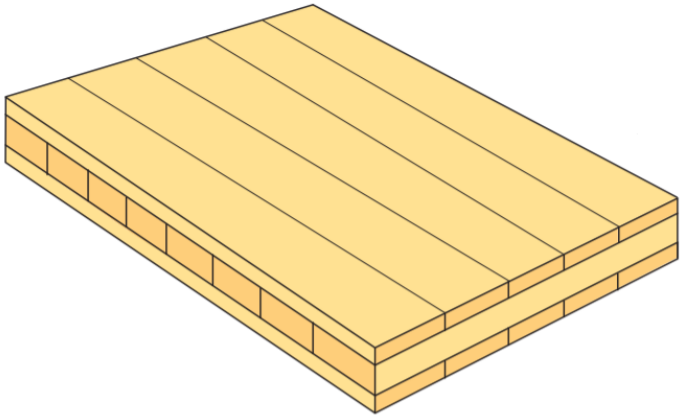

Figure 2. A 3-layer CLT slab. (Svenskt Trä, 2017)

The idea of CLT was born in the alpic region of Europe where local politicians sought an eco-friendly building material to replace concrete. The goal was to use timber instead of concrete, reducing the need to carve out ballast from ascents and riverbeds in the region. The proposition was forwarded to the top universities in Austria, and the following research resulted in CLT in the end of the 1990s [9]. Aside from the many positive environmental aspects of using a wooden building material, CLT offers a wide range of application.

The product enables a high degree of prefabrication in the building industry, with the elements themselves being prefabricated in factories and delivered to the construction site ready to be directly mounted. The wooden plates combine two functions as they can be used as supporting structures while simultaneously create room separation, either by making wall, flooring or roofing elements or by producing volume elements. It also has low self-weight which provides advantages when it comes to transport and erection. The building process is quick since CLT has full bearing capacity even before mounting in contrast to concrete elements that usually require casting and hardening. CLT can be used for many different applications but is most commonly used in the Nordic countries as load bearing elements in the form of large panels in multi-story buildings, industrial facilities, schools and houses.

3 Acoustics

Acoustics is the science of sound and is no longer limited to only air noise within the audible frequencies, but covers all media, i.e. gases, liquids and solids, and applies to all frequencies [31]. Acoustic phenomena occur in fluids when a local pressure- and density change spreads as an acoustic disturbance, an acoustic wave. Changes in local forces, stresses and strains does in a similar way create disturbances in the steady state for solid materials, which creates different wave types.

3.1 Sound pressure level

Sound is dynamic phenomena, generally referred to as oscillatory motion, where audible sound can be expressed as pressure variations in the air which are propagating as waves [12]. The sound strength can be specified as pressure where the lowest sound that most people can hear has a sound pressure of $2 \cdot 10^{-5}$ Pa, which also is called the reference sound pressure. Since humans are sensible to a wide range of sounds, usually set as the band of 20 Hz – 20 kHz, a logarithmic scale called sound pressure level (SPL) has been introduced, which is directly related to the pressure, where the sound strength is specified in decibels. The sound pressure level can be calculated as:

$$L_p = 10 \log\left(\frac{\tilde{p}^2}{p_0^2}\right) \tag{3.1}$$

Where L_p is the sound pressure level, $\tilde{p}$ is the sound pressure and p_0 is the reference sound pressure. If the sound pressure level L_p is known and the sound pressure $\tilde{p}$ is sought, a rearranging of equation 3.1 can be used:

$$\tilde{p} = \sqrt{10^{\frac{L_p}{10}} \cdot p_0^2} \tag{3.2}$$

3.2 Waves

Vibrations in fluids and solids create a pressure wave that propagates through a medium where different kinds of waves exist in different mediums. In fluids only compressional (longitudinal) waves can exist. In solids however, shear (transverse) waves also occur due to the fact that solids can store energy in shear motion. Longitudinal waves oscillate in the direction of propagation and cause longitudinal stresses which, in a finite medium such as a structure, creates lateral strains in accordance with Poisson's contraction phenomenon. Longitudinal waves in this specific form are referred as quasi-longitudinal (figure 3a). Shear waves on the other hand oscillates perpendicular to the direction of propagation and cause shear deformations (figure 3b).

Another type of wave occurring in solids of extra importance when dealing with building acoustics is the bending wave [12]. Bending waves (figure 3c) are easily excited in elements where one or two dimensions are small in relation to the wavelength of a frequency. This is often the case in building elements such as walls or floors, especially in the low-frequency range where the wavelength is longer. The wavelength is calculated as the phase velocity divided by the wave's frequency according to equation 3.3.

$$\lambda = \frac{v}{f} \tag{3.3}$$

Bending waves, like shear waves, also oscillates perpendicular to the direction of propagation and cause a rotation of the cross-section in relation to the neutral axis. The particle velocity will be in the normal direction to the propagating wave, out of the surface of e.g. a wall, making it into an efficient sound source.

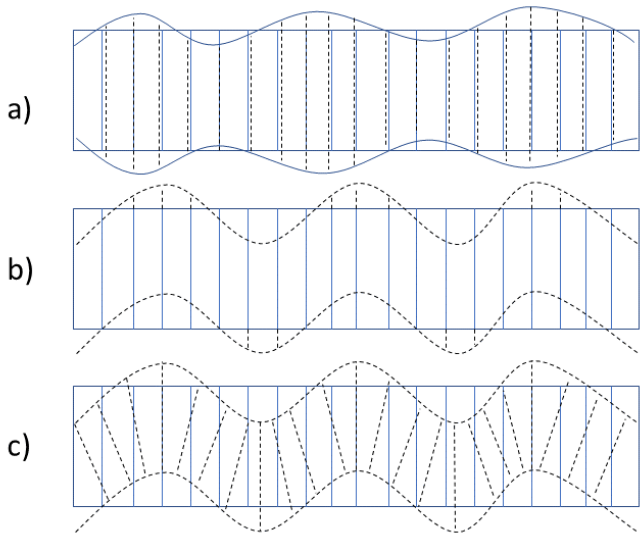

Figure 3. Different types of waves in solids. a) Quasi-longitudinal wave. b) Shear wave. c) Bending wave.

3.3 Sound transmission

Sound transmission is often divided into two groups, airborne sound transmission and structure-borne sound transmission. These two types of transmission are distinguished by the type of excitation that generates the sound.

Airborne sound transmission occurs when sound waves, from e.g. traffic noise or a loudspeaker, propagates through air and excites a component by a distributed pressure field. The component will start to vibrate, and the vibrations travel through the element which causes a pressure difference on the other side.

Structure-borne sound transmission occurs when a structural component is struck by an impact load. A typical impact load is people walking or jumping on a floor. The impact will make the component vibrate, which creates noise that will be transmitted to adjacent rooms in the same manner as for airborne sound transmission.

When a building element is set into vibration by any type of source, the path of the sound transmission can take several routes. The first and the most obvious one is directly through the element affected by the source, called direct transmission. However, the transmission can also take paths through other building elements before it radiates into a room. This phenomenon is called flanking transmission and is illustrated in figure 4. In some cases, the sound radiated from flanking transmission is even greater than the sound radiated by direct transmission. This thesis does however only deal with direct transmission, since the flanking transmission has been excluded from the standardized step sound laboratory in which the measurements are concluded.

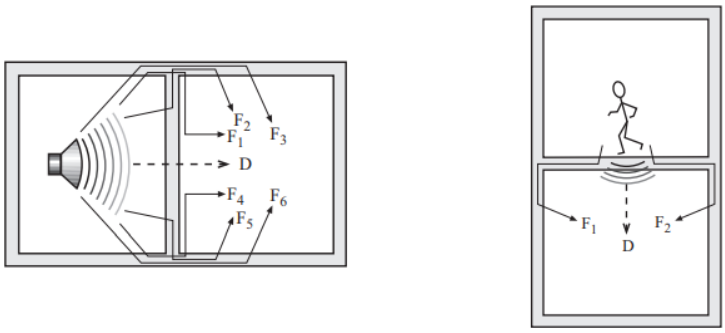

(a) Airborne sound transmission. (b) Impact sound.

Figure 4. Different transmission paths. (Negreira, 2018)

3.4 Sound insulation

Sound insulation is the overall ability to reduce the sound transmission for a building element, which also in this case can be divided in two groups; airborne sound insulation and structure-borne sound insulation. Determining the sound insulation for either case is done according to ISO 10140-2 [10] and 10140-3 [11].

Airborne sound insulation is evaluated as sound reduction index R_w and depends on the sound power on the element W_1 and the sound power transmitted through the element W_2 as:

$$R_w = 10 \log\left(\frac{W_1}{W_2}\right) \tag{3.4}$$

If the sound pressure level is measured in the rooms on either side of a wall or floor the sound reduction index for the element can be calculated as:

$$R_w = L_{send} - L_{rec} + 10 \log\left(\frac{S}{A}\right) \tag{3.5}$$

Where L_{send} is the sound pressure level in the sending room (where the sound source is located), L_{rec} is the sound pressure level in the receiving room, S is the surface of every absorption element and A is the effective absorption area of the room. The effective absorption area is often calculated from Sabines' formula by measuring the reverberation time and will be further explained in section 3.5.

It is however almost impossible to get a good sound reduction index by simply absorbing the sound energy since it instead is more effective reflecting the energy back [12]. Reflections occur when a sound ray hits a surface, where it will lose some of its energy depending on the absorption coefficient α of the surface and the remaining energy will be reflected. How the energy is reflected depends on its wavelength. If the wavelength is larger than the boundary surface the specular reflection will be dominant, where the angle of reflection is equal to the angle of incidence. If the wavelength however is smaller than the boundary surface the diffuse reflections will be dominant, also called scattering. Illustration of the phenomena is shown in figure 5.

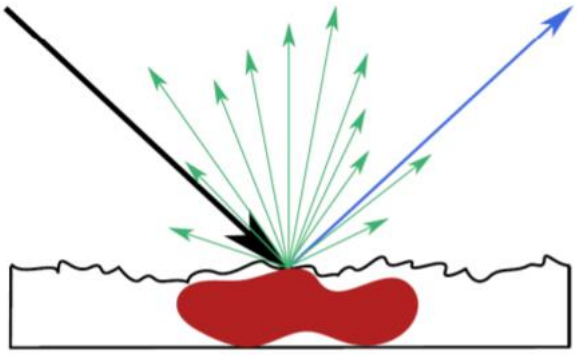

Figure 5. Illustration of absorption (red), specular reflection (blue) and diffuse reflection (green) of incident sound energy. (Negreira, 2018)

The incident sound energy (black) will thus partly be absorbed (red), specularly reflected (blue) and diffusely reflected (green) according to figure 5. The proportion of the energy being absorbed, specularly reflected and diffusely reflected is equal to 1 if summed.

Structure-borne sound insulation is evaluated as impact sound level L_n and depends on the sound pressure level in the receiving room L_r and the effective absorption area in the receiving room A as:

$$L_n = L_r + 10 \log\left(\frac{A}{10}\right) \tag{3.6}$$

The tapping machine is employed as excitation source for the impact sound evaluation according to the ISO standards. The standardized tapping machine hits the floor once every 0.1 seconds and has 5 steel cylinders which alternatively hits the floor.

When checking the overall sound insulation of a room the weakest link in the construction has a big impact and it is therefore for instance important to avoid leakage between construction elements [13].

3.5 Reverberation time

The reflections of sound waves emitted by a source that occur after 50 ms is defined as reverberation. As described in chapter 3.4 a sound wave will lose some of its energy when it hits an element due to absorption. A soundwave in a room bounces multiple times the energy will decay exponentially, whereas the sound pressure level will decay linearly. The reverberation time T_{60} is defined as the duration required for the space-averaged sound energy density in an enclosure to decrease by 60 dB after the source emission has stopped [14]. It can however be evaluated on smaller dynamic ranges other than 60 dB, such as 20 dB and 30 dB, and extrapolated to a decay time of 60 dB, due to the linear decay assumption of the SPL. The reverberation time is entitled T_{20} if based on 20 dB and T_{30} if based on 30 dB.

The reverberation time has become a common parameter to evaluate the acoustic performance of rooms since it highly affects a person's experience in it, controlling parameters such as speech intelligibility and noise level. Two regulated methods can be used to evaluate the reverberation time; interrupted noise method and impulse response method [14].

- The interrupted noise method employs a broadband or band-limited noise, such as pink noise, as the source to acoustically excite the room. By abruptly interrupt the noise the SPL decay curve is recorded, from which the reverberation time is subsequently derived.

- The impulse response method is performed by exciting the room with an impulse noise, with e.g. a cap gun. The measurement equipment will react to the impulse noise and start recording the SPL decay from which the reverberation time is subsequently derived.

The reverberation time can also be calculated according to Sabine's formula:

$$T_{60}(f) = 0.16\frac{V}{A(f)} \tag{3.7}$$

Where $T_{60}(f)$ is the reverberation time, V is the volume of the room and $A(f)$ is the total effective absorption area of the room. The total effective absorption area can be calculated as:

$$A(f) = \sum_{i=1}^{n} S_i \alpha_i(f) \tag{3.8}$$

Where S_i is the surface in the room with the absorption coefficient α_i. Calculating the total effective absorption area with equation 3.8 would require knowledge, or estimations, regarding the absorption coefficient of each surface. An alternative method is to instead measure the reverberation time and calculate the total effective absorption area using Sabine's formula according to:

$$A(f) = 0.16\frac{V}{T_{60}(f)} \tag{3.9}$$

3.6 Sound radiated from a vibrating plate

The sound pressure level in a room resulting from a vibrating plate is dependent on the actual modal pattern of the plate, which is further determined by the modes and their individual vibration amplitudes. This indicates that the radiated sound cannot be calculated from solely the dimensions and material properties of the plate. The excitation source must also be known since each mode will depend on how the structure is driven by the source. From there, the velocities of the plate vibrating in a simple harmonic way can be calculated as:

$$v_z(x,y) = \hat{v}\sin\left(\frac{n_x \pi x}{a}\right)\sin\left(\frac{n_y \pi y}{b}\right) \qquad 0 \le x \le a,\ \ 0 \le y \le b \tag{3.10}$$

Where $\hat{v}$ is the velocity amplitude, n_x and n_y are the modal numbers in x- and y-direction, a and b are the length and width of the plate. If the velocities of the surface of the plate are known the velocity level L_v can be calculated according to equation 3.11. Just as the sound pressure level this is a logarithmic scale, that is directly related to the velocity, where $v_0 = 1 * 10^{-9}\, m/s$ is the velocity reference level and $\tilde{v}$ is the root mean square of the velocity amplitude.

$$L_v = 20\log\left(\frac{\tilde{v}}{v_0}\right) \tag{3.11}$$

$$\tilde{v} = \frac{\hat{v}}{\sqrt{2}} \tag{3.12}$$

Kurzweil [22] investigated the relationship between a floor slab's acceleration and subsequent sound pressure level in the room, creating a widely used reasonable estimation. The estimation can in terms of velocity level be simplified [23] to:

$$L_p = L_v - 27 \tag{3.13}$$

Where L_v is the vertical velocity level of the plate.

4 Structural dynamics

This chapter will deal with the governing theory of structural dynamics that explains how a structure responds to vibrations and clarifies important terms such as natural frequencies, resonance and damping. Vibrations arise in a system when it is subjected to dynamic forces or moments. These forces can be present due to the direct impact on elements of the structure or due to sound pressure.

4.1 Single degree of freedom system

The simplest dynamic system is the single degree of freedom (SDOF) system. The number of degrees of freedom (DOFs) of a system is defined as the number of independent displacements required to define its position or motion. A damped SDOF system can be represented by the classic mass-spring-damper system, illustrated in figure 6. The motion of this system can be described with Newton's second law of motion:

$$m\ddot{u}(t) + c\dot{u}(t) + ku(t) = p(t) \tag{4.1}$$

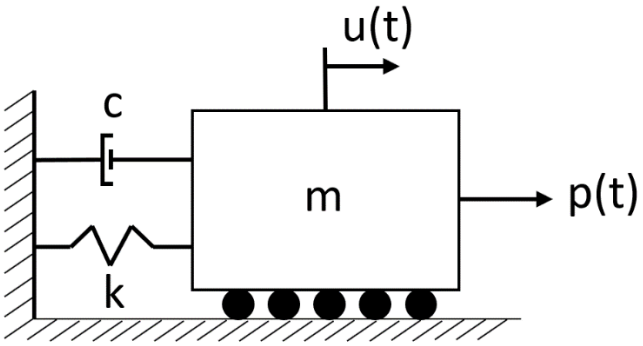

Figure 6. A single degree of freedom system.

Here all motions are assumed to be in x-direction, the damper and spring to be massless and the mass to be lumped. The forces acting on the mass in this system are the elastic resisting force $f_s = ku$, the damping resisting force $f_d = c\dot{u}$ and the external force $p(t)$. The coefficient k is the spring stiffness, c is the viscous damping coefficient and m is the mass. The time dependent displacement $u(t)$ is obtained by solving equation 4.1. If a harmonic force $p_0 \sin\omega t$ is introduced the equation can be written as:

$$m\ddot{u} + c\dot{u} + ku = p_0 \sin\omega t \tag{4.2}$$

Where p_0 is the amplitude and ω is the loading frequency. Solving this equation with the initial conditions of $u = u(0)$ and $\dot{u} = \dot{u}(0)$, the particular solution can be written as:

$$u_p(t) = C sin\omega t + D cos\omega t \tag{4.3}$$

Where

$$C = \frac{p_0}{k} \frac{-2\zeta\, \omega/\omega_n}{[1-(\omega/\omega_n)^2]^2 + [2\zeta(\omega/\omega_n)]^2} \tag{4.4}$$

$$D = \frac{p_0}{k} \frac{1 - (\omega/\omega_n)^2}{[1 - (\omega/\omega_n)^2]^2 + [2\zeta(\omega/\omega_n)]^2} \tag{4.5}$$

The coefficient ζ is the damping ratio. The complementary solution is given by:

$$u_c(t) = e^{-\zeta\omega_n t}(A cos\omega_D t + B sin\omega_D t) \tag{4.6}$$

where

$$\omega_D = \omega_n\sqrt{1 - \zeta^2} \tag{4.7}$$

In total, the solution (particular plus complementary) is then written as:

$$u(t) = e^{-\zeta\omega_n t}(A cos\omega_D t + B sin\omega_D t) + C sin\omega t + D cos\omega t \tag{4.8}$$

The parameters A and B can be determined by differentiating, using the initial conditions of the displacement u_0 and velocity $\dot{u}(0)$. The particular solution describes the transient response and the complementary solution describes the force response. The transient response, or the free vibration, depends on the initial displacement and velocity while the force response, or steady state response, is present due to the applied force independently of the initial conditions. With time the transient response decays while the force response remains, hence called the steady state response.

4.2 Deformation response factor

The ratio between the amplitude of the dynamic deformation u_0 and the static deformation $(u_{st})_0$ is called the deformation response factor Rd and it is defined as:

$$R_d = \frac{u_0}{(u_{st})_0} = \frac{1}{\sqrt{[1 - (\omega/\omega_n)^2]^2 + [2\zeta(\omega/\omega_n)]^2}} \tag{4.9}$$

As it can be observed from this equation, when the forcing frequency ω coincides with the natural frequency ω_n the deformation response factor R_d grows to infinity if no damping is present ($\zeta = 0$). This is the phenomena of resonance. A system can have several resonant frequencies, as many as the number of DOFs of the system, and they are defined as the loading frequency that yields the largest response amplitude.

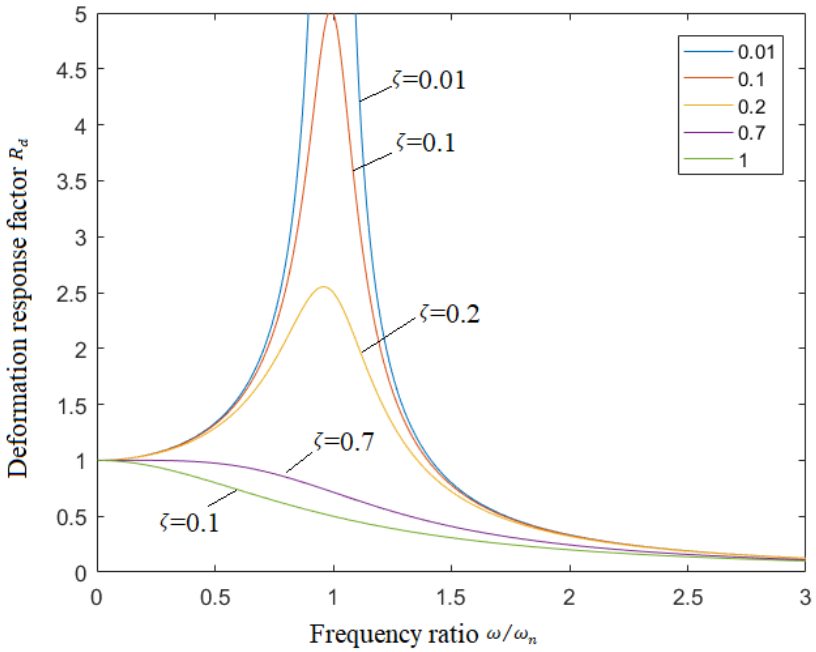

Figure 7. Deformation response factor for a damped system excited by harmonic force with different damping.

4.3 Free vibration

If a structure is set into motion, i.e. disturbed from its static equilibrium, and then allowed to vibrate freely without applying any additional external force, the structure is set into free vibration. The frequency in which said structure will vibrate in is called a natural frequency and the rate of which the motion decreases is controlled by the damping. The experimental data obtained when setting a structure into free vibration can therefore be used to determine the natural frequency and damping ratio of a system [12]. The natural frequency depends only on the mass and the stiffness of the system. A stiffer system will have a higher natural frequency and a shorter period time while a heavier system will have a lower natural frequency and a longer period time according:

$$\omega = \sqrt{\frac{k}{m}} \tag{4.10}$$

$$f = m\ddot{u} \tag{4.11}$$

If no damping is present, a system set into free vibration would theoretically continue to oscillate infinitely. However, damping is always present to some degree in a real system. Solving the equation of motion with free vibration $p(t) = 0$ yields:

$$m\ddot{u} + c\dot{u} + ku = 0 \tag{4.12}$$

Dividing the equation with m gives:

$$\ddot{u} + 2\zeta\omega_n\dot{u} + \omega_n^2 u = 0 \tag{4.13}$$

Using the definition of ω_n from equation 4.10 together with

$$\zeta = \frac{c}{2m\omega_n} = \frac{c}{c_{cr}} \tag{4.14}$$

gives

$$c_{cr} = 2m\omega_n = 2\sqrt{km} = \frac{2k}{\omega_n} \tag{4.15}$$

Where c_{cr} is the critical damping coefficient and ζ the damping ratio. A system is considered overdamped if $\zeta > 1$, underdamped if $\zeta < 1$ and critically damped if $\zeta = 1$. In the realm of civil engineering, where calculations are made regarding structures such as dwellings, dams and bridges, systems fall into the category of underdamped. This type of structures usually has a damping ratio below 10% [15]. The damped natural frequency is then given by:

$$\omega_D = \omega_n\sqrt{1-\zeta^2} \tag{4.16}$$

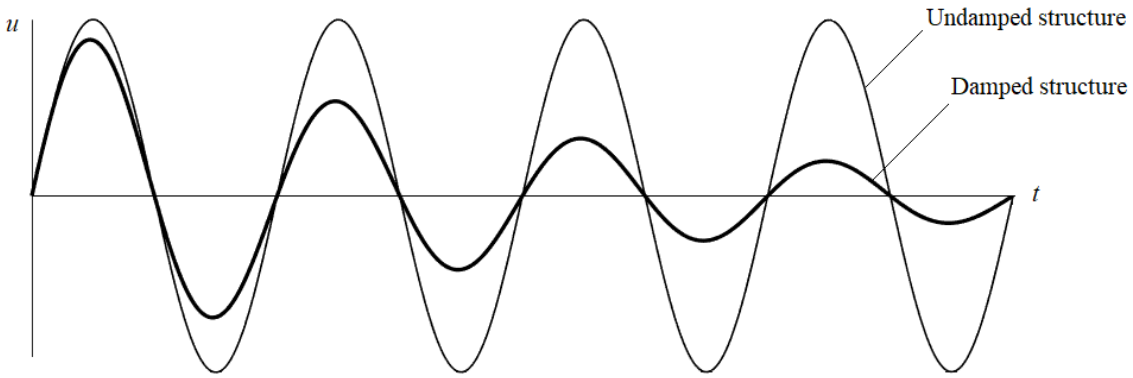

Figure 8. Amplitude response of a damped and undamped structure.

In comparison with the undamped system, the damped systems amplitude is reduced in every cycle. Damping reduces the natural frequency from ω_n to ω_D, but this effect is negligible for damping ratios below 20%, which includes most structures [15].

4.4 Damping

When a component or a system of several components is set into oscillatory motion, mechanical energy dissipates in every cycle. This dissipation of energy occurs due to friction where mechanical energy converts into other forms of energy, e.g. thermal. This phenomenon is known as damping, often categorized as structural or material damping.

Structural damping is the loss of mechanical energy due to friction between different members in a system, typically within joints. Material damping is the loss of mechanical energy due to internal friction within the material itself. Damping is usually a non-linear phenomenon but can be modelled as linear under the assumption of small oscillations and small damping [21], suitable for acoustic analyses. There are two main mathematical damping models, the viscous model and the hysteretic model, with the latter being the most common. Damping is often amplitude dependent, i.e. dependent on the force applied. Note that damping is an elusive

property that should be determined experimentally for a structure. There are different methods to achieve this, one of them being the half-power-bandwidth method.

4.4.1 Half-power-bandwidth method

By examining the experimental data of the dynamic response of a system, the damping coefficient in resonant frequencies can be obtained. The damping of the system is determined by examining the sharpness of the amplitude peak. By plotting the response versus the frequency and identifying at what frequency the resonance amplitude begins and ends, together with the peak value of said amplitude, using the following equations unfolds the damping coefficient.

$$2\zeta = \frac{\omega_b - \omega_a}{\omega_n} \tag{4.17}$$

$$\zeta = \frac{\omega_b - \omega_a}{2\omega_n} = \frac{f_b - f_a}{2f_n} \tag{4.18}$$

The damping coefficient in every resonant frequency can by this method be obtained from experimental data and later be used in numerical models. However, the damping coefficient obtained by use of the half-power bandwidth method is very sensitive to the peak amplitude value and therefore highly dependent on the resolution of the transfer response and sampling rate [21].

4.5 Mode shapes

When a structure is resonating in a natural frequency, it moves in a specific pattern called an eigenmode Φ_n. The movement of the structure can be described mathematically with

$$\boldsymbol{u}(t) = q_n(t)\Phi_n \tag{4.19}$$

where $q_n(t)$ is the time variation of the displacements and can be described with:

$$q_n(t) = A_n cos\omega_n t + B_n sin\omega_n t \tag{4.20}$$

A_n and B_n are constants that can be determined with the initial conditions of the movement. Using the equation of motion (equation 4.1) together with equation 4.19 and 4.20 the following relationship is obtained:

$$[-\omega_n^2 \boldsymbol{m}\Phi_n + \boldsymbol{k}\Phi_n]q_n(t) = 0 \tag{4.21}$$

This results in an equation with two solutions, the trivial solution where the system is not in motion and $q_n(t) = 0$, or the particular solution where $\boldsymbol{k}\Phi_{\mathrm{n}} = \omega_n^2 \boldsymbol{m}\Phi_n$. The latter is an eigenvalue problem with the solution:

$$\det[\boldsymbol{k} - \omega_n^2 \boldsymbol{m}] = 0 \tag{4.22}$$

Solving this equation gives the eigenfrequencies of the system and once they are known, the eigenmodes can be determined by insertion into the particular solution:

$$\boldsymbol{k}\Phi_{\mathrm{n}} = \omega_n^2 \boldsymbol{m}\Phi_n \tag{4.23}$$

5 The finite element method

The finite element method has during the last decades become the main technique to analyze physical phenomena in the field of structural, solid and fluid mechanics. Physical phenomena within these fields are modelled by differential equations where analytical methods often are insufficient. By using a numerical approach, the solution can be approximated at discrete points. The essence of the finite element method is that instead of seeking an approximation for a complex differential equation describing a physical problem over a whole region, the region is divided into smaller parts and each part is approximated in a simpler fashion. These smaller parts of a region are the so-called finite elements. The approximation estimates how the quantity of interest, e.g. stress, varies over the element. With the assumption that the value is known at some location of the element, an interpolation is then carried out to find the value at other locations. The approximation is usually a polynomial and can be either linear or of higher order, depending on the problem at hand. When the behavior of each finite element is determined, the behavior of the entire body can be determined by assembling and connecting all elements [24].

5.1 Elements

The finite elements can be modelled in different ways by using different element types. The choice of element type is highly dependent on the problem and the sought result. Elements are categorized in a broader fashion as line, area and volume elements and more specifically by the number of nodes.

1D elements are sufficient for problems dealing with value variation in only one direction such as trusses. 2D elements are perhaps most commonly used for plate and shell problems where plane stress or plain strain can be assumed. The 3D volume elements are commonly used to model solids. Tetrahedral elements are less precise than hexahedral but are useful for modeling complex geometries. For simple solid geometries the hexahedral brick element is the optimal choice.

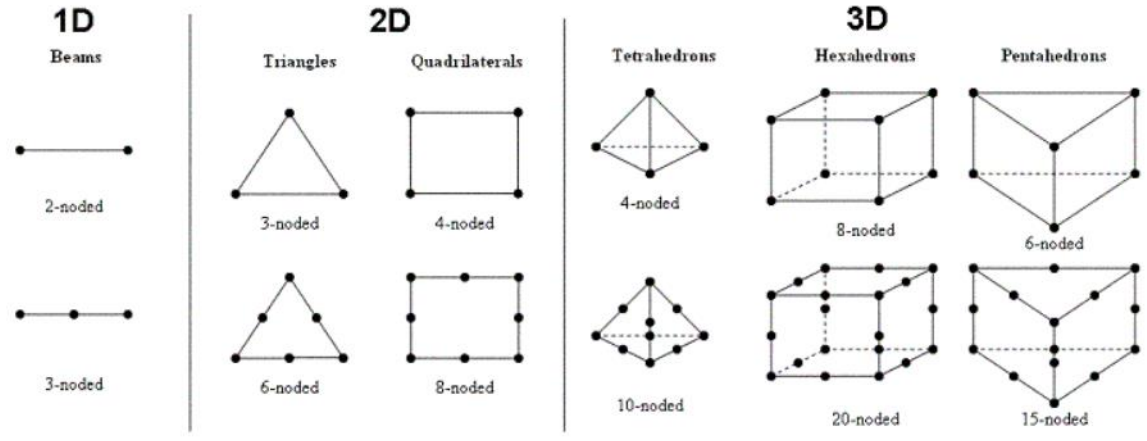

Figure 9. Different types of finite elements.

5.2 Mesh

The collection of all finite elements describing the region of the problem is called mesh. By reducing the size of each element, the mesh is refined, where a finer mesh yields more precise results but also requires more computational effort. By investigating the convergence of

element size and accuracy of results (relative error), the adequate element size can be determined. The rule of thumb of an acoustic- or structural dynamic problem is to consider 6 to 8 nodes per wavelength [25], meaning that the highest frequency of interest governs the size of the elements.

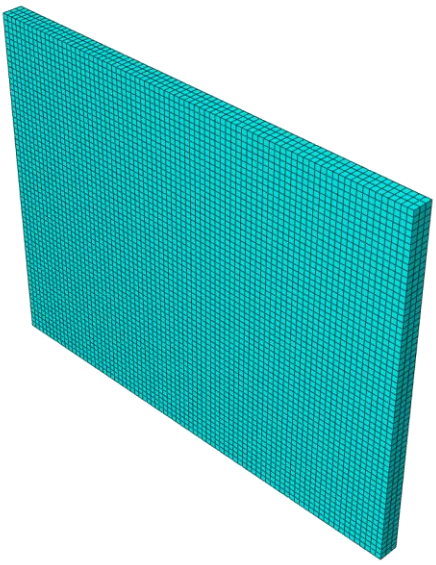

Figure 10. The mesh of a plate.

5.3 Model validation

The FE model can be validated by comparing the simulation results and the measurement results. Different methods exist to validate models, with two techniques commonly used being the modal assurance criterion (MAC) and the normalized relative frequency difference (NRFD), which are adopted in this thesis. A common way to obtain measurement results when dealing with structural dynamic problems is by use of an experimental modal analysis (EMA).

5.3.1 Experimental modal analysis

The experimental modal analysis (EMA) method is commonly employed to determine the dynamic properties of the structure, such as the eigen-frequencies, mode shapes as well as damping ratios. In order to measure the dynamic response of a structure it is excited by a stimulus. This is usually done with a modal hammer, that excites the structure with an impulse load, or with one or several shakers that excites the structure periodically. The response is commonly measured as accelerations and is recorded with one or several accelerometers at a number of locations, which has to be strategically placed around the structure in order to reveal its mode shapes. One strategy is to first try to estimate the shape of the modes of interest, making sure not to place the accelerometers in positions of zero displacements, known as *nodes*. The mode shapes are determined with the help of several transfer functions of the structure. With the information gathered it is then possible to construct a model of the structure which then can be used to predict the response of an arbitrary excitation [12]. In this thesis, the results of the EMA are considered as references to accurately calibrate the material parameters of the FE model.

Different experimental protocols can be used, depending on different excitation points (input) and different acceleration measurement point (output).

- Single Input Single Output (SISO) is a measurement system where the structure is excited at a single location and the response is recorded at a single location.
- Singe Input Multiple Output (SIMO) is a measurement system where the structure is excited at a single location and the response is recorded at multiple locations simultaneously.
- Multiple Input Single Output (MISO) is a measurement system where the structure is excited at multiple locations and the response is recorded at a single location.
- Multiple Input Multiple Output (MIMO) is a measurement system where the structure is excited at multiple locations and the response is recorded at multiple locations simultaneously. This method is commonly used for complex structures where multiple inputs are required in order to sufficiently distribute the excitation energy along the structure.

Hammer testing was used for the EMA in this project, which also is the most common one since it is quick and relatively cheap. Multiple Input Multiple Output (MIMO) was considered most suitable for this case in order to get the excitation energy sufficiently distributed along the structure. The measurements are set up with a software where each hitting- and accelerometer position is recreated virtually. The test specimen is then excited in a specific order according to the software, recording the accelerations of the specimen in multiple positions for every hammer hit. In this thesis, five accelerometers were used to record each hitting position.

5.3.2 Modal assurance criterion

One of the results obtained from a FEM analysis are the mode shapes. In order to validate an analytical model, the shape of the modes can be compared with measured results. This can be done in a simpler, basic fashion by eye, or more analytically by a technique known as the modal assurance criterion (MAC) which determines the correlation.

$$MAC = \frac{\left|(\Phi_i^a)^T(\Phi_i^b)\right|^2}{\left|(\Phi_i^a)^T(\Phi_i^a)\right|\left|(\Phi_i^b)^T(\Phi_i^b)\right|} \tag{5.1}$$

The result is the normalized square product of the eigenvectors obtained from experimental (Φ_i^a) and analytical (Φ_i^b) results, where a MAC value of 0 means that there is zero correlation between the mode shapes and a MAC value of 1 is total correlation [26].

5.3.3 Normalized relative frequency difference

The normalized frequency difference is an indicator showing the discrepancies in frequency between an analytical model and measurements. Each eigen-frequency (i) is compared from the different cases (a, b). A low value as possible is desirable, with 0 being no difference in frequency between the two cases.

$$NRFD_i[\%] = \frac{[f_{a_i} - f_{b_i}]}{f_{b_i}} * 100 \tag{5.2}$$

To validate a predictive tool both the NRFD and MAC methods should be used together. Using only one of them alone does not give enough information since a high MAC correlation could be achieved in the wrong frequencies, and vice versa [30].

6 Parameter study

Wood displays large variations in material parameters as described in chapter 2. Therefore, the parameters must be verified for the specific specimen under study with measurements in order to create an accurate model. In this thesis, the response of a five-layer CLT slab was analyzed with the Experimental Modal Analysis (EMA), as described in section 5.3.1, and the Abaqus model was calibrated with the help of these results. The model was calibrated by tweaking the parameters in the model until the response matched the measured response.

6.1 Measurement procedure

The experimental modal analysis measurements were set up by placing a CLT slab on two steel beams and restraining it with clamps, locking it in place in the vertical direction, to mimic simply supported conditions (figure 11). The dimensions of the slab was 1.5x4 m^2.

Figure 11. Measurement setup.

In order to assure that the accelerometers were not placed in nodes of deformation modes, a position along a wave with minimum amplitude, a grid was created (figure 12). The red lines denote theoretical node positions for the first 4 modes in the transverse and longitudinal direction. The black lines represent the grid on which the accelerometers were placed, effectively avoiding the nodes. The intersections of the black lines are also the hitting positions of the impact hammer. The grid was drawn onto the actual slab and measurements were carried out accordingly. The CLT slab was struck 3 times in each position, and an average response was calculated with the software.

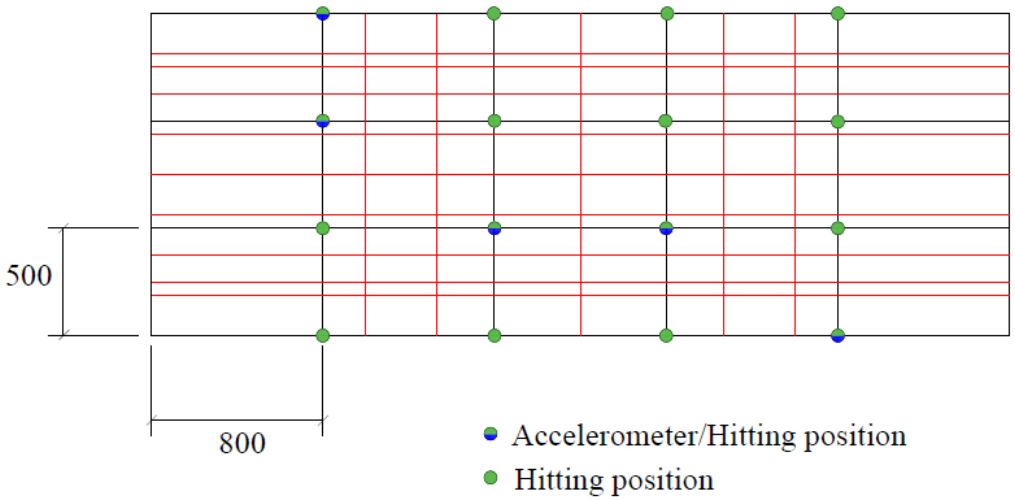

Figure 12. The grid dictating accelerometer placing and hitting positions.

The accelerometers used for the measurement were piezoelectric Bruel & Kjaer DeltaTron type 4507-001 [16]. These accelerometers record accelerations in one direction, depending on how they are oriented. Vertical accelerations were recorded for this study. The hammer was a Bruel & Kjaer modal sledgehammer type 8208 [17], which is designed to excite and measure impact forces on medium to large structures. Different tips can be attached to the hammer, varying from hard to soft, controlling the amplitude and decay of the impact and frequency response. The medium tip was chosen for the measurements in this thesis to make sure that resonance frequencies up to 200 Hz were excited.

Figure 13. Bruel & Kjaer accelerometer (left), Bruel & Kjaer modal hammer (middle), hammer tip diagram (right)

The data output from the accelerometers and impact hammer was recorded with the FFT analyzer tool Bruel&Kjaer PULSE LabShop [18] software, and post processed in BK Connect 2018 [19]. When analyzing the frequency response function (FRF) obtained from the EMA, an auto function in BK connect was used in order to find the eigenmodes for each resonance frequency. Different input data could be modified such as the frequency span, which was set to 210, and the number of iterations which usually was set between 40 and 50. When doing this some peaks could be seen that obviously represented an eigenmode but was not picked up by the auto function. In those cases, a narrower frequency span had to be used in order to isolate the peak and capture the response.

Several measurements with different boundary conditions (no clamping, clamped on both sides, clamped on one side) were performed, showing that the clearest response in terms of resonance peaks and distinguishable mode shapes were found when the CLT slab was clamped on both sides. The best result obtained from the measurements, in terms of clear resonance peaks and modal shapes, is displayed in terms of resonance frequencies in table 1 and modal shapes in figure 14.

Table 1. Modes and corresponding frequencies, obtained from the EMA.

Mode	Frequency (Hz)
1	19,97
2	32,45
3	56,66
4	74,1
5	93,07
6	124,43
7	170,37
8	191,69

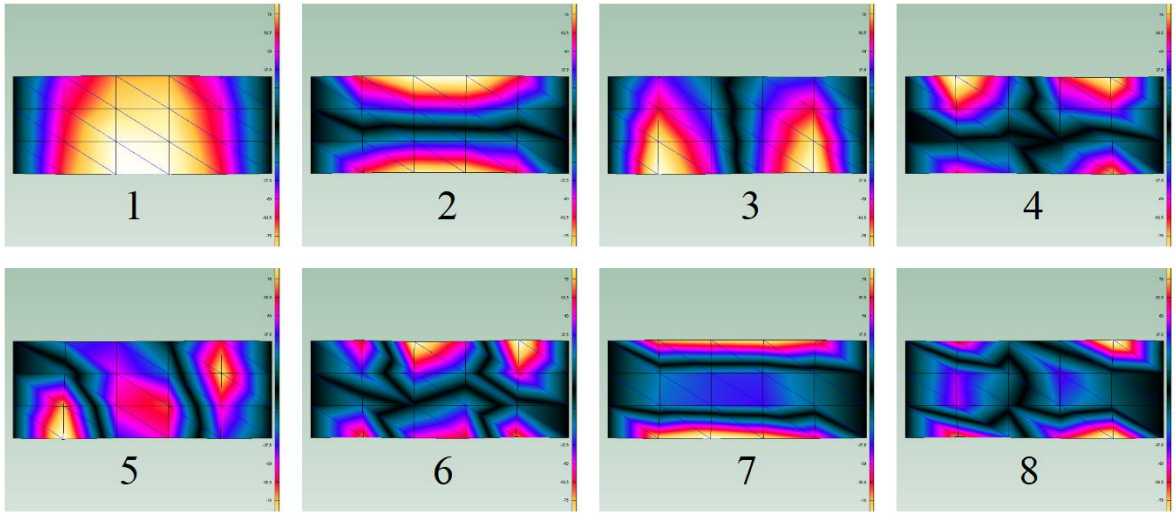

Figure 14. Captured modal shapes obtained from the EMA.

6.2 Model

When modelling the CLT, there are two main routes to take. The first one would be to model each layer separately, defining the material properties as of a collection of planks and orienting them perpendicularly in each layer. This method will however bring many variables, since every plank would likely display parameter discrepancies, and every layer subsequently. Calibrating such a model is tedious work, where the question would arise to which layer to adjust.

The other alternative is to create a homogenous model where the material properties are not the actual properties of an isolated wood specimen, but rather an average, weighted in the direction of the CLT where the majority of the layers are parallel. In a five-layer CLT, three of the layers will be parallel in one direction, with two of the layers perpendicular. In this thesis, the homogenous model was chosen. Previous research regarding modelling of CLT has shown

that the homogenous model is sufficient and that the effect of the adhesive (glue) can be neglected [20].

This way of defining the material parameters leads to a model in which the parameters will be different depending on the number of layers. A five-layer CLT slab will have more evenly distributed parameters than a three-layer, simply due to the fact that the parameters will even out in the x- and y-direction. In a three-layer CLT, 2/3 of the layer will be in the stiff direction whereas a five-layer CLT will have 3/5. The obvious drawback of this approach is that the parameters cannot be reused if a CLT slab with a different number of layers is to be assessed. With the varying nature of woods material parameters, a reuse of parameters between different models is however not optimal and these should be investigated independently. The models in this thesis were created with solid 20 node brick elements, interpolated quadratically.

6.2.1 Boundary conditions

The boundary conditions applied in the model mainly controls the stiffness of the structure. With more rigid boundary the stiffness increase and the resonance frequencies increase subsequently in each mode. This adds to the complexity of the model calibration, where uncertainties arise from the interaction between the boundary conditions and the magnitude of the material parameters. If the stiffness appears too high, it is not an easy way to be sure whether the boundaries are too rigid or the material parameters are too stiff. In the parameter study the choice was made to use line-tie boundaries on both sides of the CLT slab, in a simply supported fashion where one side is clamped in three directions x, y, z and the other side in the two directions y, z (figure 16).

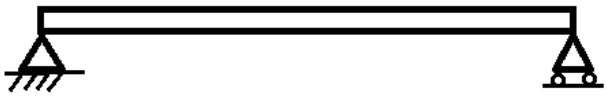

Figure 15. Schematic figure of a simply supported beam.

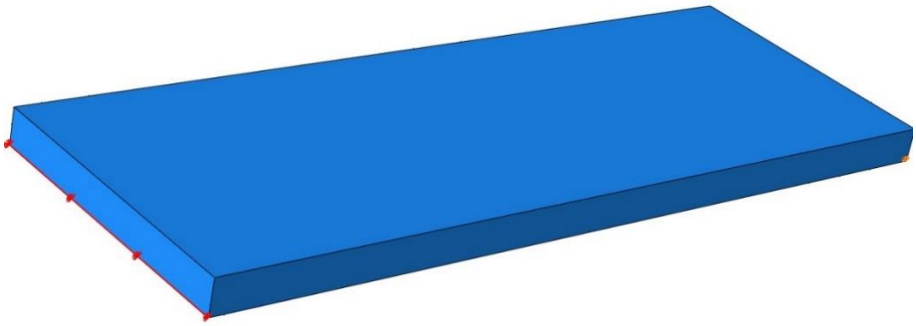

Figure 16. The boundary conditions applied as lines in Abaqus.

6.2.2 Parameter verification

The results from the experimental modal analysis determines the resonance frequencies and mode shapes of the CLT. By comparing the mode shapes, the order of the modes and the resonance frequencies obtained from the EMA measurements with the initial Abaqus model, the material parameters and boundary conditions are tweaked in the model to match the measurements. Each parameter impacts the results differently and interact with each other.

The parameters were calibrated by starting with values obtained in other research regarding homogenous modelling of CLT [20] and tweaked in order to match the specific CLT slab analyzed in this thesis. The parameters were calibrated in an iterative fashion, by either increasing or decreasing each parameter with 20%, until the sum of the NRFD for all eight modes reaches a point where further adjustment are unfavorable. The sum is considered decisive, since changing a parameter can be beneficial for one mode but disadvantageous for others. The best match was found using the parameters in table 2.

Table 2. Starting values and calibrated values for the material parameters.

Parameter	Starting values	Calibrated
Denisty	515	515
E_1 [Pa]	8,24E+09	5,99E+09
E_2 [Pa]	3,12E+09	3,24E+09
E_3 [Pa]	3,67E+08	1,27E+09
ν_{12}	1,29E-02	0.05
ν_{13}	6,30E-02	0.03
ν_{23}	1,22E-02	0.3
G_{12} [Pa]	6,90E+08	6,90E+08
G_{13} [Pa]	1,73E+08	1,73E+08
G_{23} [Pa]	9,86E+07	1,18E+08

The resulting NRFD using the calibrated material parameters according to table 2 is displayed in figure 17. The sum of the NRFD for all eight modes with these parameters is 33.87%. As can be seen in the figure, mode 1 and 5 contribute largely to the sum.

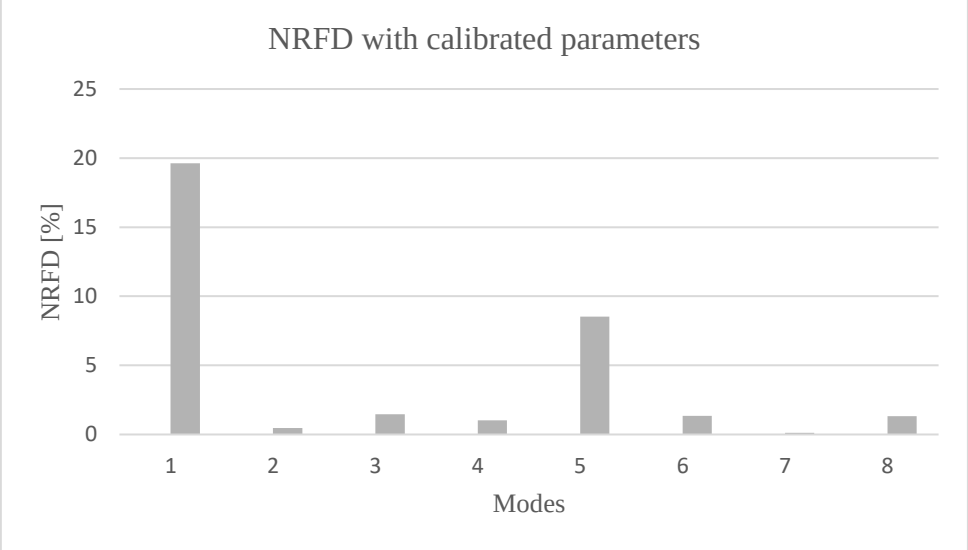

Figure 17. The normalized frequency difference for each mode, using material parameters according to table 2.

Table 3 displays the effect of increasing and decreasing each parameter with 20% in relation to the chosen values (table 2). As can be observed from this table, any change of magnitude of the parameter values in table 2 are disadvantageous to the sum of the NRFD, concluding that these parameters are optimal under the chosen boundary conditions. The modulus of elasticity has the largest impact on the frequencies, while the poissons ratio has the least. Individual modes can however be improved at the cost of a worse NRFD sum. An argument can be made that a more evenly distributed NRFD in each mode is better than having a few modes (in this case mode 5 and 1) that deviate largely.

Table 3. The effect of increasing/decreasing each material parameter by 20% in relation to the finalized values.

Mode	1	2	3	4	5	6	7	8	**Sum NRFD**
Base value	19,63	0,46	1,46	1,01	8,52	1,34	0,11	1,33	33,87
E_1 decreased	27,49	2,65	9,37	4,67	1,11	2,36	1,50	0,45	49,60
E_1 increased	12,72	1,51	5,12	2,04	14,49	4,28	1,59	0,16	41,91
E_2 decreased	19,63	0,49	1,46	1,05	8,51	1,30	5,56	5,53	43,55
E_2 increased	19,63	0,46	1,48	1,03	8,50	1,33	7,43	4,41	44,27
E_3 decreased	19,83	1,26	2,38	2,25	7,11	0,38	1,46	0,44	35,13
E_3 increased	19,48	0,22	0,71	0,00	9,71	2,80	1,63	0,16	34,71
G_{12} decreased	19,63	5,95	1,48	4,21	8,50	0,69	1,16	1,16	42,79
G_{12} increased	19,63	4,25	1,46	1,73	8,50	3,16	1,88	0,80	41,42
G_{13} decreased	20,28	2,37	3,79	3,54	4,89	2,50	1,36	0,94	39,67
G_{13} increased	19,18	0,92	0,18	0,72	11,19	4,20	1,70	0,51	38,59
G_{23} decreased	19,63	1,11	1,48	1,71	8,50	1,05	2,09	3,41	38,98
G_{23} increased	19,63	0,00	1,48	0,57	8,50	1,49	4,21	2,30	38,19
ν_{12} decreased	19,63	0,49	1,46	1,04	8,51	1,30	1,51	0,21	34,17
ν_{12} increased	19,63	0,43	1,45	0,99	8,54	1,37	1,70	0,13	34,23
ν_{13} decreased	19,63	0,46	1,46	1,01	8,52	1,34	1,63	0,00	34,06
ν_{13} increased	19,63	0,46	1,46	1,01	8,52	1,35	1,63	0,01	34,07
ν_{23} decreased	19,63	0,46	1,48	1,04	8,50	1,32	1,55	0,13	34,11
ν_{23} increased	19,63	0,46	1,46	1,01	8,52	1,33	1,58	0,09	34,10

6.2.3 Convergence

In order to get reliable results from the FEM calculations the mesh convergence had to be checked, i.e. making sure the model yields the same result even if the number of elements are increased. The model was tested with different number of elements and the resulting resonance frequencies for the first eight modes was compared. Figure 18 displays the eigenfrequency for mode 7 with increasing number of elements in the mesh. Convergence is considered achieved with 7200 elements. The convergence in the remaining modes can be found in appendix A.

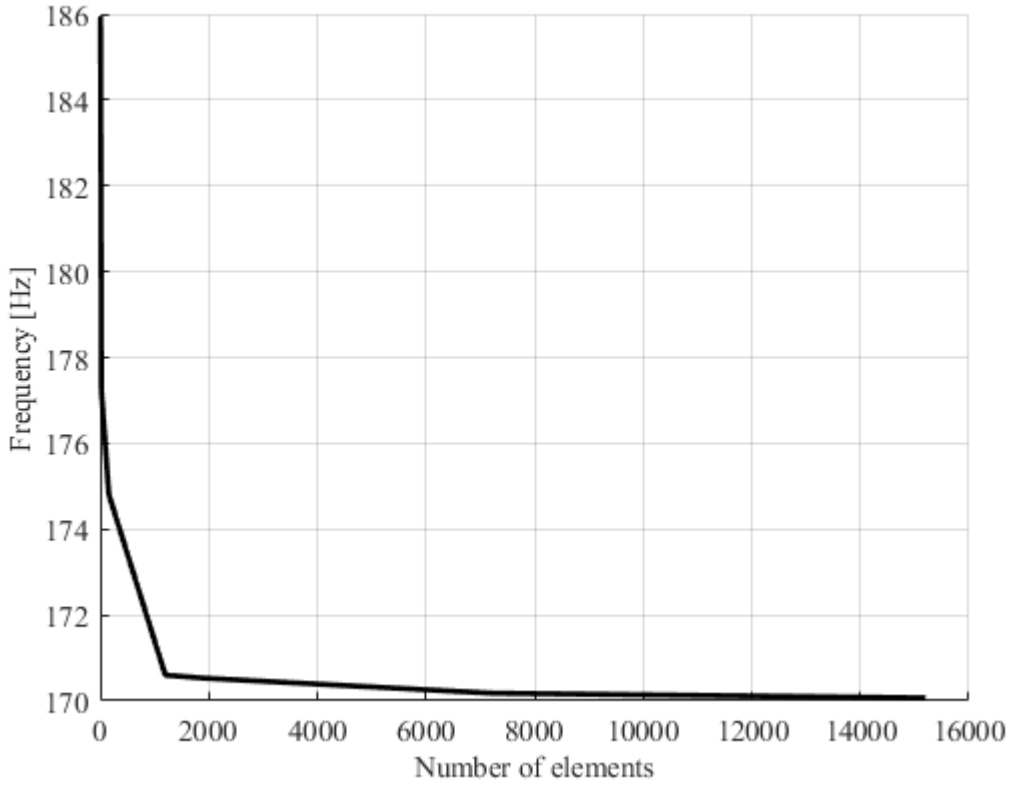

Figure 18. Convergence in space for mode 7.

6.2.4 Mode shapes

The resulting mode shapes when running the Abaqus model in a frequency sweep from 0-200 Hz are displayed in figure 19. Thirteen modes were captured. The EMA results (chapter 6.1) revealed 8 modes, and these 8 modes can easily be picked out from the 13 obtained in Abaqus. There can be several reasons to why more modes appear in the model, which will be discussed later on in the thesis (chapter 8). However, by ignoring the unwanted modes and comparing the remaining ones to the measured results, a match was found that can be seen by comparing figure 20 and 21.

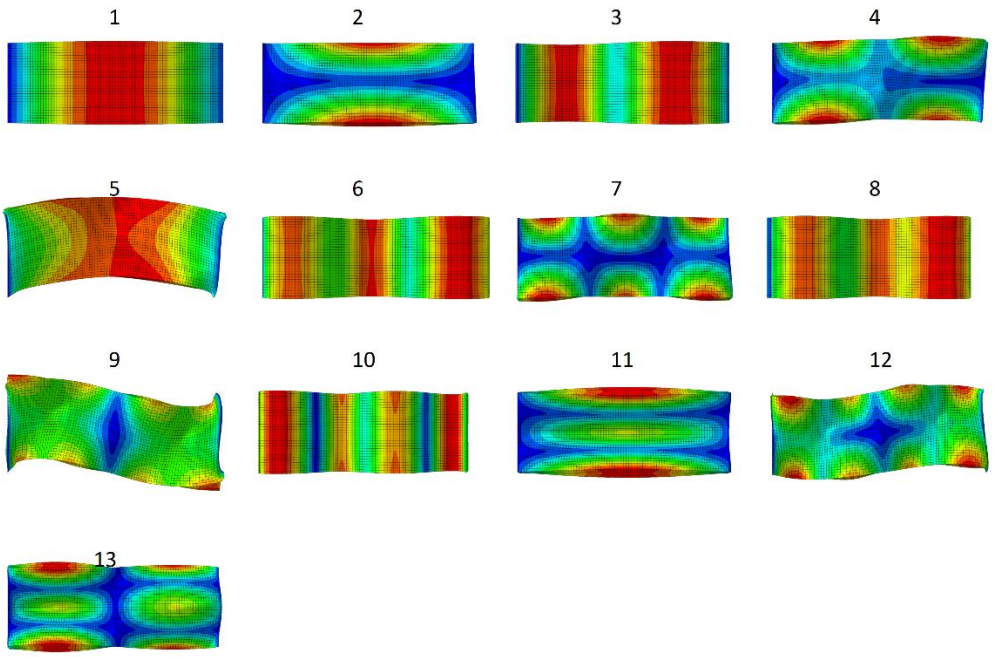

Figure 19. All 13 modal shapes captured in Abaqus.

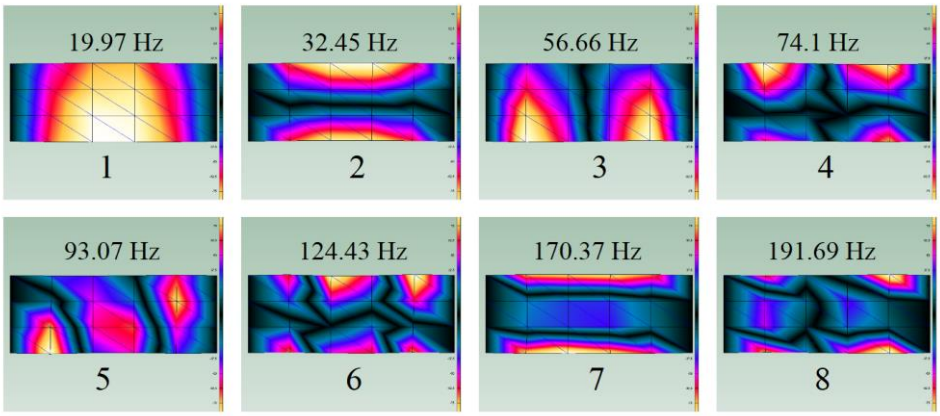

Figure 20. Modal shapes together with frequencies obtained from the EMA measurements.

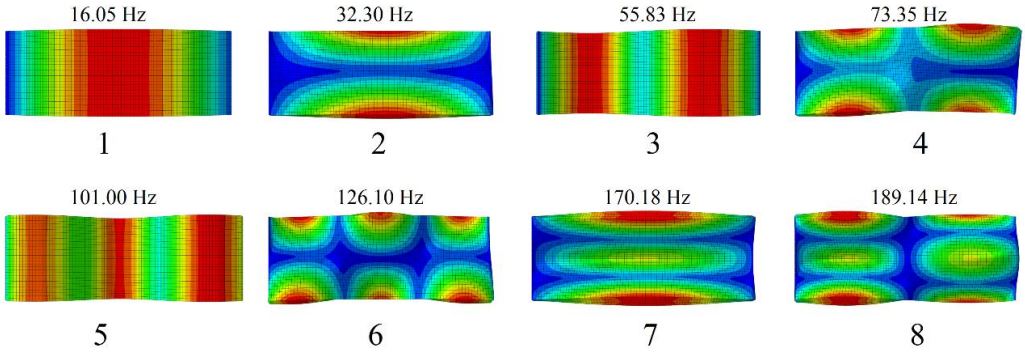

Figure 21. Matching 8 modal shapes together with frequencies obtained from the Abaqus model.

6.3 Modal assurance criterion

Running a MAC analysis, comparing the 8 modal shapes from measurements with the corresponding mode shapes from Abaqus, the result displayed in table 4 was obtained. The MAC-value, as explained in chapter 5.3.2, indicates total correlation between the analytic and measured modal shapes if the value is 1. The table shows a strong correlation in most modes, where mode 5 deviates with a lower correlation. This mode also showed a large NRFD in chapter 6.2.2, indicating that this mode was not captured correctly

Table 4. Correlation between the Abaqus modal shapes and measured modal shapes.

Modes	1	2	3	4	5	6	7	8
1	0,985	0,006	0	0	0,019	0,001	0,179	0,008
2	0,013	0,986	0,001	0,006	0,007	0,014	0	0,002
3	0	0,001	0,897	0,073	0,0023	0,051	0,001	0,131
4	0	0,005	0,089	0,887	0,149	0,034	0,005	0,008
5	0,007	0,001	0,037	0,003	0,675	0,04	0,001	0,063
6	0	0,001	0,001	0,001	0,086	0,845	0,001	0,004
7	0,145	0	0	0,001	0,001	0,004	0,969	0,0026
8	0,001	0	0,12	0,005	0,003	0,017	0,01	0,849

7 Sound reduction index model

To create and verify a FE model that predicts the airborne sound insulation of CLT, certain measurements must be performed. A five-layer CLT slab, from the same producer and batch as the one previously analyzed (chapter 6), was measured in a sound transmission lab. There are three objectives of these measurements:

1. Determining the damping of the structure in the specific setting during the measurements to use in the model in chapter 7.3
2. Determining the sound pressure in the room during the measurements to use as load to calculate the sound reduction index in chapter 7.4
3. Determining the sound reduction index to compare with the results from the model in chapter 7.4

7.1 Airborne sound measurement procedure

The apparent sound reduction index for the five-layer CLT wall was determined by conducting measurements in an acoustic lab facility in LTH. The facility is normally used as a step sound lab to investigate impact sound transmission of flooring components, designed so that no flanking transmission is present. The size of the aperture is 3x4 m^2, requiring two individual CLT slabs to cover it. The connection between these two slabs is unknown and not accounted for in this thesis. An assumption was made that the connection is rigid, and the slab can be analyzed as one homogenous part. The CLT was placed horizontally in the slot, effectively dividing the room volume into two. The upper floor was utilized as the receiving room and the bottom floor as the sending room (figure 22). The volume of the receiving room is 79.87 m^2. The sound reduction index is calculated with equation 3.5, and in order to do so the sound pressure level must be measured in both the sending and receiving room when noise is emitted. The effective absorption area must also be determined by conducting reverberation time measurements in the receiving room and making use of Sabine's formula (equation 3.9).

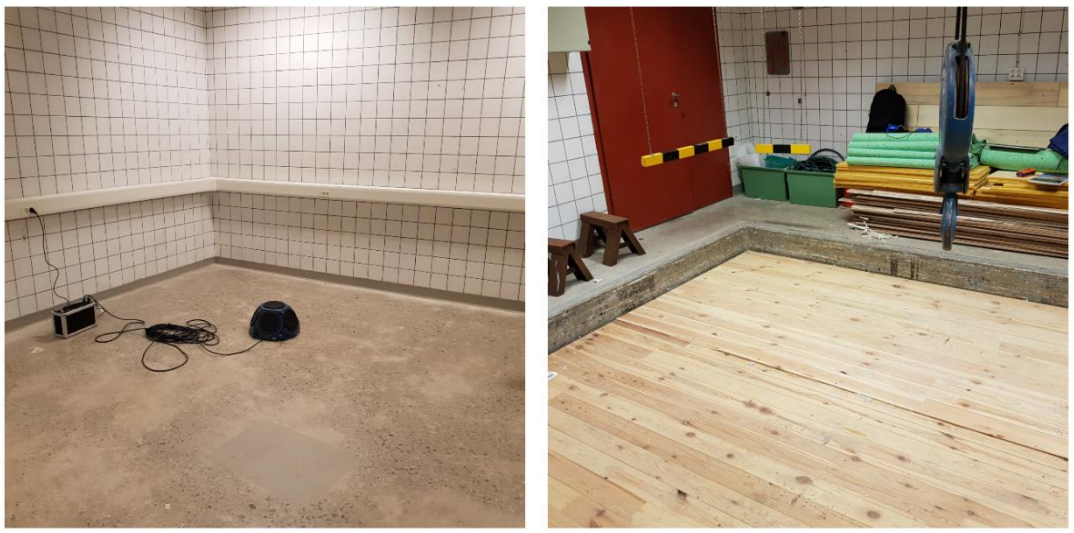

Figure 22. Transmission lab. Sending room (left) and receiving room (right).

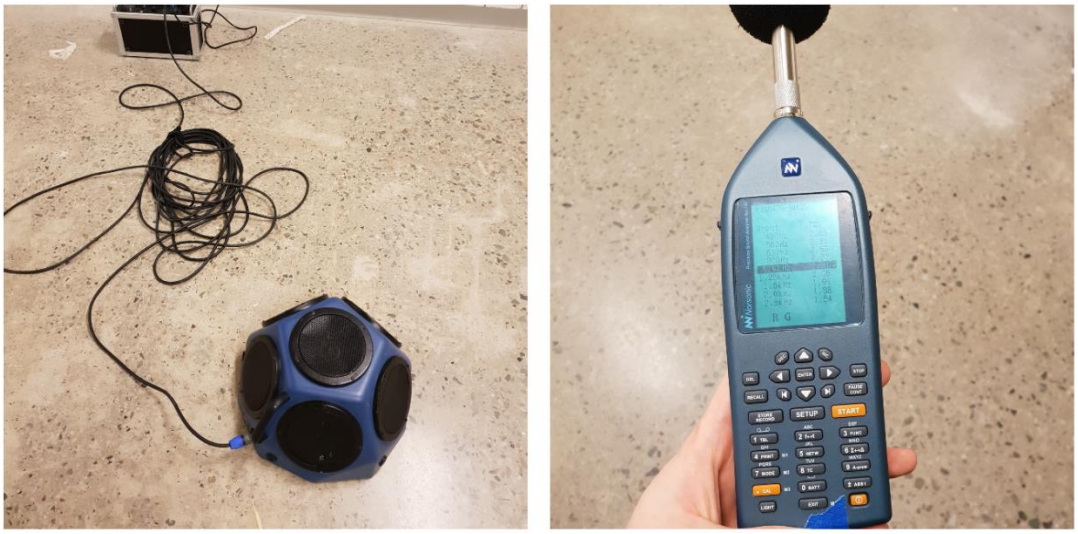

Figure 23. Measurement equipment. Loudspeaker (left) and sonometer (right).

7.1.1 Sound pressure level

First, the sound pressure level L_p was recorded in both the sending and the receiving room when pink noise was emitted by a loudspeaker. The measurement procedure, in accordance with ISO 10140-4 [29], was to use three fixed loudspeaker positions together with five microphone recordings for each position. A Norsonic140 sonometer was used to record the sound pressure level in 1/3 octave bands. Once the sound pressure levels were recorded, an average of the fifteen measurements in both the receiving and sending room was calculated in each frequency band. The results can be observed in figure 24.

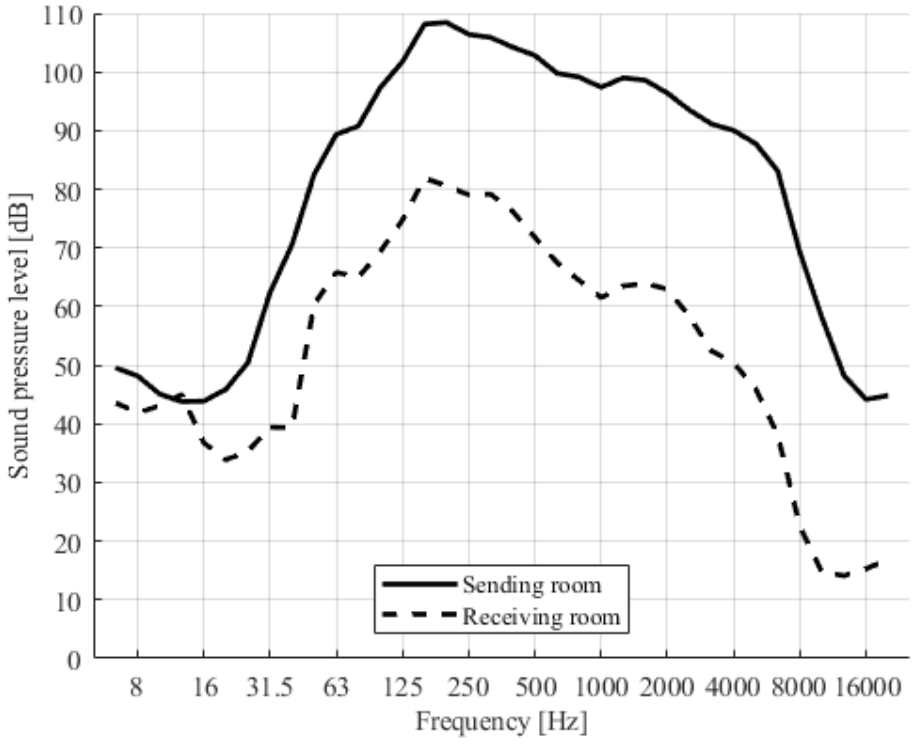

Figure 24. Recorded average sound pressure level in sending and receiving room.

7.1.2 Sound pressure

A root mean square (RMS) of the sound pressure $\tilde{p}$ was calculated based on the recorded sound pressure levels L_p (chapter 7.1.1) according to equation 3.2. This pressure, displayed in table 5, was used as the load to predict the sound reduction index in chapter 7.4.

Table 5. Calculated sound pressure.

Freq. (Hz)	$\tilde{p}$ (Pa)
6,3	0,006003
8	0,005133
10	0,003595
12,5	0,003098
16	0,003121
20	0,003936
25	0,006663
31,5	0,026284
40	0,067665
50	0,267935
63	0,586629
80	0,690817
100	1,473545
125	2,447353
160	5,113246
200	5,280763

7.1.3 Reverberation time

The reverberation time was measured in the receiving room in 1/3 octave bands with the interrupted noise method. The loudspeaker was placed in two positions in the receiving room and the reverberation time was recorded in 5 different positions for each speaker position. When using the Norsonic140, the reverberation time is recorded from 50Hz and upwards. The average reverberation time in each frequency band was calculated. The results can be observed in figure 25.

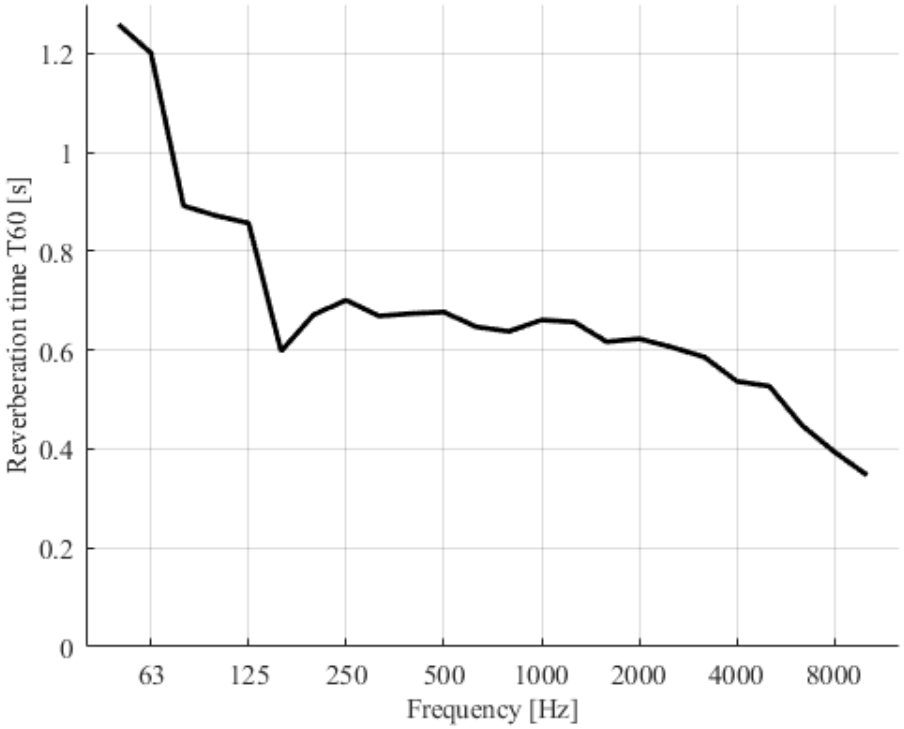

Figure 25. Measured average reverberation time in the receiving room.

The receiving room's dimension is 5.1x5.8x2.7 m^3. By using Sabine's formula (equation 3.9), the effective absorption area of the receiving room was determined for each frequency in the 1/3 octave band and can be seen in figure 26.

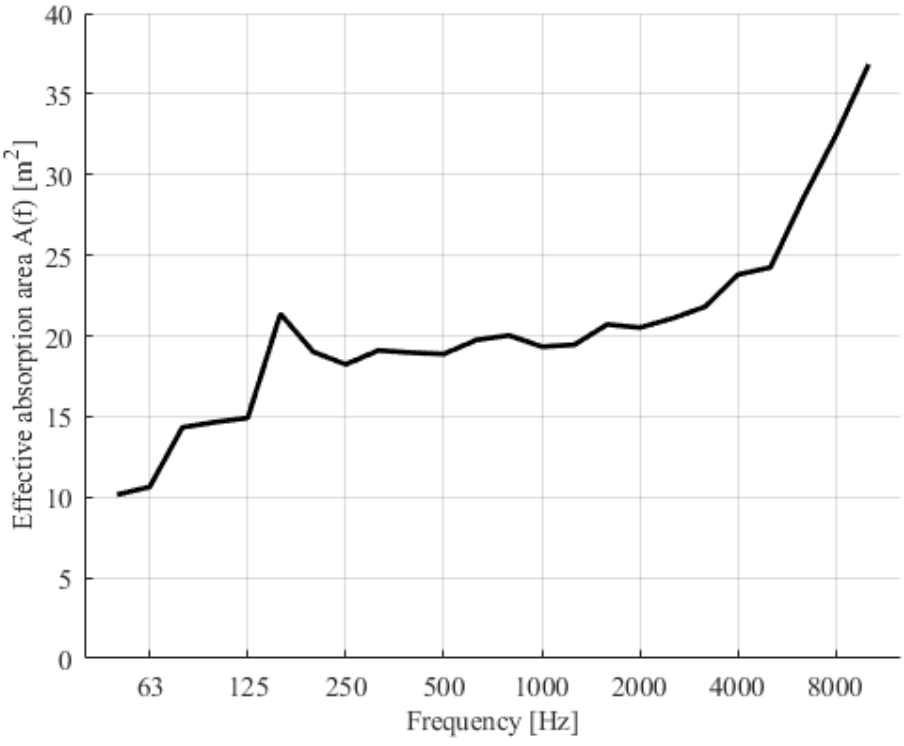

Figure 26. Calculated absorption area in the receiving room.

7.1.4 Sound reduction index

The apparent sound reduction index was calculated (equation 3.5) using the average values of the SPL in the sending and receiving room, the effective absorption area together with the surface area of the CLT. The result is displayed in figure 27.

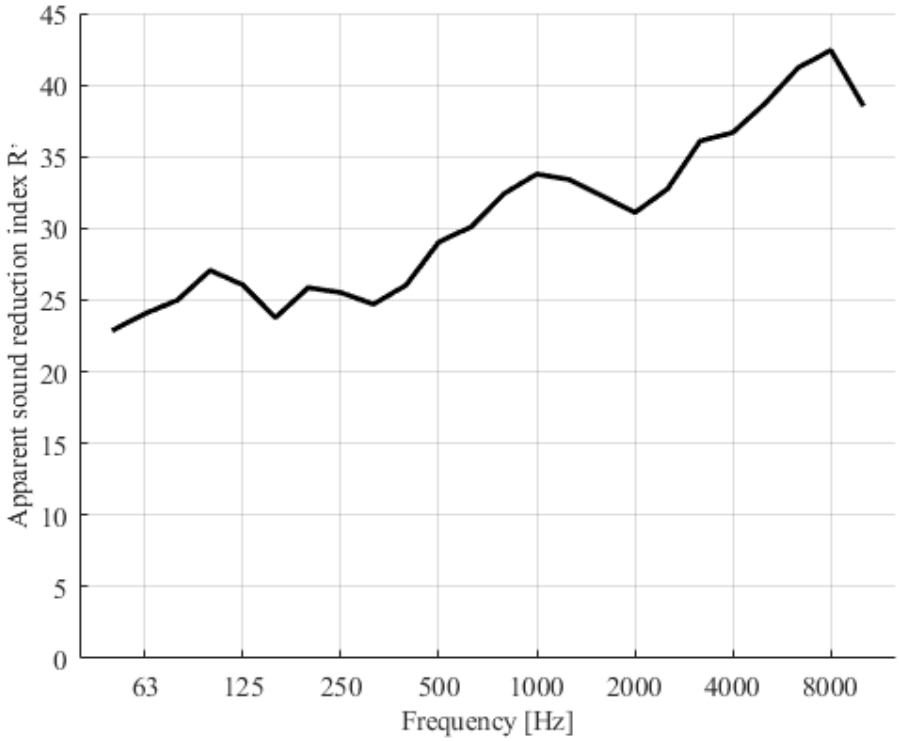

Figure 27. Calculated apparent sound reduction index.

7.2 Damping measurements

The total damping of a structural member consists of both material- and structural damping. This makes the damping a case specific parameter, since the same member will have different damping depending on how and where it is placed in the global structure. In order to replicate the sound insulation of the five-layer CLT wall from the measurements with a FEM-model, the damping was investigated in the transmission lab (figure 28).

Figure 28. Damping measurement setup in the transmission lab.

Four accelerometers were placed on the CLT slab and set into vibration by transient blows with a hammer. The response was recorded by the accelerometers and the damping calculated with the Bruel & Kjaer software BK connect [19]. The software uses an algorithm based on the half-power bandwidth method, giving the critical damping factor for each mode. The results are displayed in table 6. Since only vertical accelerations are recorded, the damping belongs to vertical modes. As is shown in chapter 7.3, three rigid body modes appear in the Abaqus model. Mode 1 in table 6 is therefore analogous to mode 4 in the Abaqus model.

Table 6. Measured critical damping coefficient.

Mode	Damping
1	5,68978
2	3,41859
3	6,8434
4	3,99921
5	2,34631
6	4,69692
7	1,79993
8	3,62273
9	3,129
10	2,36221
11	3,05959
12	1,86636
13	1,8518

7.3 Modelling

In this chapter the model was run in two steps, first in a frequency sweep to determine the modes and corresponding eigenfrequencies up to 200 Hertz and secondly in a modal steady state step. The second step is where the load is applied, a uniformly distributed pressure of 1 Pa over the whole surface area. The response of the structure is calculated in the second step based on the modal behavior retrieved in the frequency sweep. From this response velocities were extracted and multiplied with the pressure amplitudes recorded in the sending room in chapter 7.1.1. The resulting velocity levels were then used to calculate a sound pressure level inside the room with Kurzweils approximation (equation 3.13). The calculated sound pressure was then compared to the measurement data. By applying the same load as the one active during the sound pressure measurements, a correct model should yield similar results in terms of sound pressure levels. Damping does however play a big role on the results, since it directly influences the velocity amplitudes.

The approach to create the sound reduction model was to use the material parameters of a five-layer CLT according to chapter 6.2.2 and damping according to chapter 7.2, in a new model of a CLT slab with the same dimensions as the one analyzed during the sound transmission measurements. The damping was applied in Abaqus as direct modal damping in the steady state modal step. Once again, the CLT is modeled as homogenous with 20-node solid brick elements. The slab rests on the edges of the aperture without any mounting (figure 28), which was modeled as a simply supported plate according to figure 29.

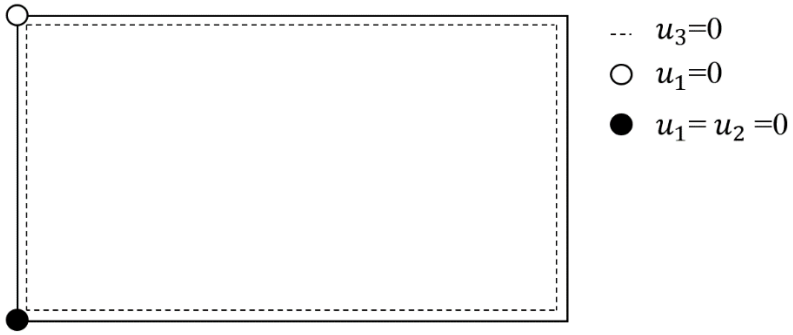

Figure 29. Schematic figure of the boundary conditions of a simply supported plate.

Running a frequency step in Abaqus reveals the modes and eigenfrequencies of the model, presented in figure 30 and table 7. The three first modes are rigid body modes and are misleading since they are not realistic to occur, but a consequence of the boundary conditions where the x and y directions are fixed in single points. In order to not have these modes contributing to the result they were “damped out” by applying 100% damping in these modes in the subsequent modal step. In theory, these modes will not contribute anyway since the movement in these modes is in the xy-plane and will therefore not contribute with velocities in the z direction, which is the analyzed direction.

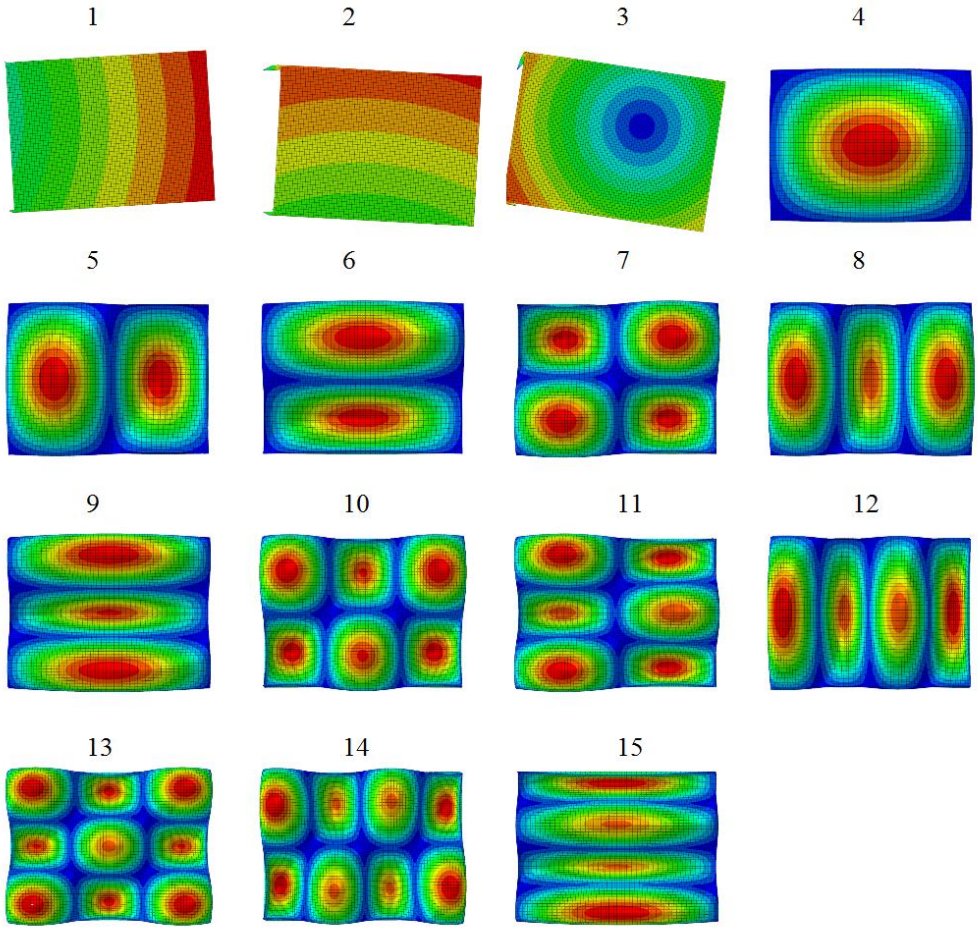

Figure 30. All 15 captured modal shapes in Abaqus.

Table 7. Eigenfrequencies obtained in Abaqus.

Mode	Frequency
1	7,58
2	15,34
3	19,89
4	28,76
5	63,85
6	74,54
7	96,16
8	113,72
9	132,38
10	135,99
11	146,93
12	167,43
13	176,61
14	184,29
15	192,18

A convergence check in space was also made for this model and can be found in appendix B.1. The number of elements necessary was determined to 15000. Since this model was run in a second modal steady state step, a convergence check regarding the number of increments was also performed. The increment convergence is determined from the response due to loading, where the increment size governs the resolution of the amplitude peaks. If not enough increments are used, maximum values of the amplitude peaks might be missed. By running the model with 50, 100, 200 and 600 increments and calculating the sound pressure level from the velocity amplitudes in the resonating modes, the variation of the results was analyzed. The increment convergence is analogous to the one for element size, assuring that the results does not differ considerably with smaller increments. The necessary amount of increments was determined to 200 and the convergence in the first resonance mode is displayed in figure 31. Convergence check for the remaining modes can be found in Appendix B.2.

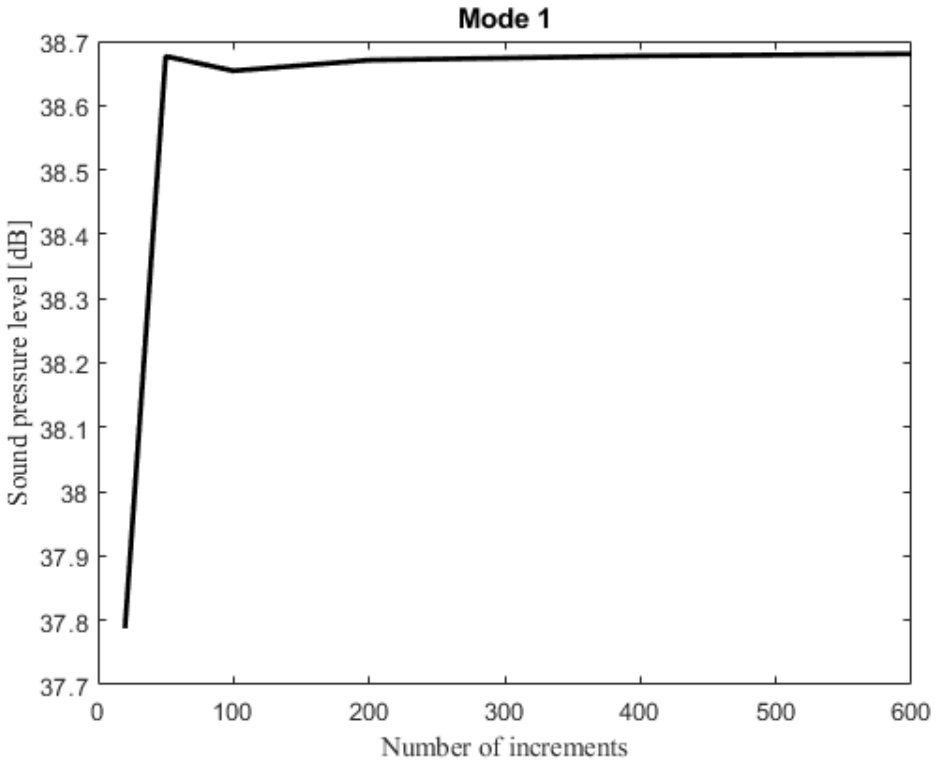

Figure 31. Increment convergence in the first resonance mode.

When the model was run through the modal steady state step with the pressure of 1 Pa, a frequency response function (FRF) was obtained by extracting the velocities from nodes on the surface. This resulting FRF was considered as a representative response, linearly proportional to any arbitrary pressure. An example of how the FRF looked, with velocities extracted from 143 nodes scattered over the surface, is shown in figure 32.

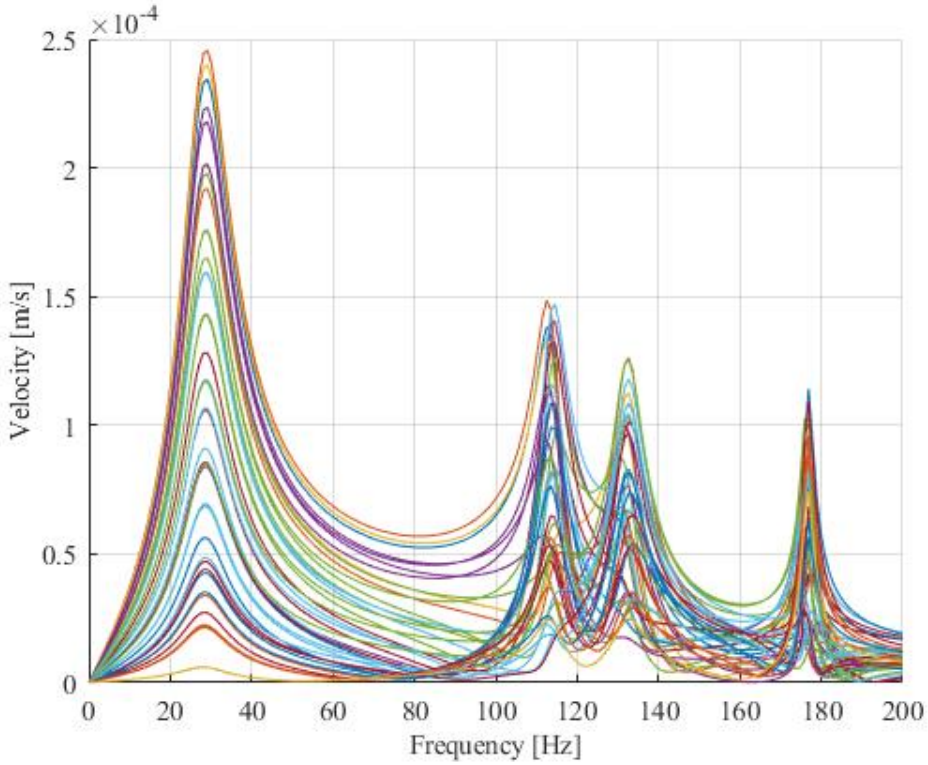

Figure 32. Frequency response function when the model is exposed to a pressure load of 1 Pa. The response is plotted for 143 nodes scattered over the surface.

7.4 Predicting the sound reduction index

By multiplying the amplitude peaks of the FRF with the pressure levels in corresponding frequencies recorded in the sending room during the transmission measurements (section 7.1.2), the response of the slab is mimicked. The average peak velocity was calculated by finding the maximum amplitude value of the velocity in each node of the surface near the four excited resonance frequencies. This was achieved by exporting the velocity response data to Matlab [27] where a script was created to find the maximum velocities within certain intervals around the resonance frequencies. An average velocity over the whole surface was then calculated at each resonance frequency. The average will differ with the number of nodes in which the velocities are extracted, since more nodes will yield a better representation of the surface. With the mesh size of 0.05 and the use of 20-node brick elements, the surface holds 14681 nodes. Figure 33 displays the FRF with the velocities extracted from all nodes of the surface, in the form of magnitude when the model is run with the measured damping according to section 7.2.

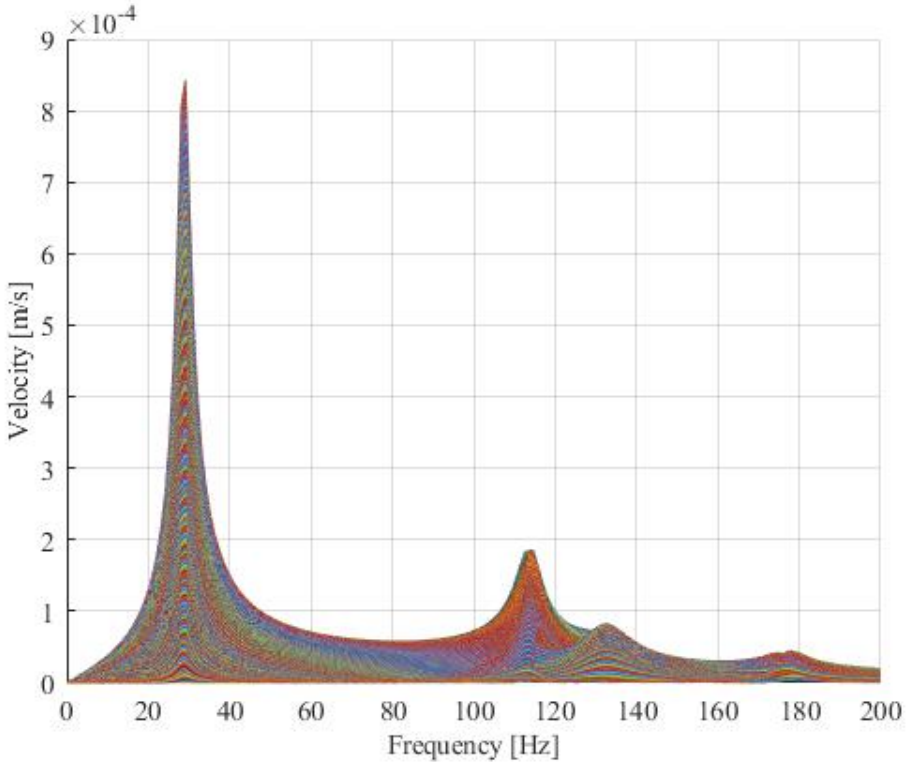

Figure 33. Frequency response function when the modell is exposed to a pressure load of 1 Pa, using modal damping according to measurements. The response is plotted for all 14681 nodes of the surface.

Note that the response displayed in figure 32, 33 and 34 is completely changed when multiplied with the measured pressure (table 8). The proportions of the peaks change, where the first peak is reduced with approximately 98% while the second is doubled, third is tripled and the fourth is 5 times larger. As can be seen clearly in figure 34, four resonance frequencies are excited at 29, 114, 132 and 177 Hz. The measured sound pressure level is however recorded in 1/3 octave bands (figure 24), so the sound pressure level (L_p) and sound pressure ($\tilde{p}$) was interpolated (table 8) to get a value in these frequencies.

Table 8. Interpolated sound pressure level and sound pressure.

Freq. (hz)	29	114	132	177
L_p (dB)	38.474	72.613	76.377	81.129
$\tilde{p}$ (Pa)	0.0187	2.019	2.981	5.184

The response, in terms of velocity in a selected number of nodes over the surface, is used to calculate a velocity level (equation 3.11). The velocity level is then converted to a sound pressure level L_p by Kurzweil's approximation (equation 3.13). The resulting sound pressure level, using the measured damping, does however not give a perfect match to the measured sound pressure levels with values displayed in table 9. The sound pressure level is too high in the first resonance frequency and too low in the fourth. The middle frequencies are relatively accurate.

Table 9. Measured and predicted sound pressure level using the measured damping according to chapter 7.2.

Freq. (hz)	29	114	132	177
L_p measured (Pa)	38.474	72.613	76.377	81.129
L_p measured damping (Pa)	46.419	75.000	73.381	72.040

In order to get a better match, the damping was modified according to table 10. The resulting FRF is displayed in figure 34. As can be seen in the table and according to previous discussions in chapter 7.3, the first 3 modes are dampened out completely.

Table 10. The applied damping in Abaqus.

Mode	Measured	Modified
1	1	1
2	1	1
3	1	1
4	0.0569	0.15
5	0.0342	0.05
6	0.0684	0.05
7	0.0400	0.05
8	0.0235	0.03
9	0.0470	0.03
10	0.0180	0.03
11	0.0362	0.015
12	0.0313	0.01
13	0.02362	0.006
14	0.0306	0.006
15	0.0187	0.006

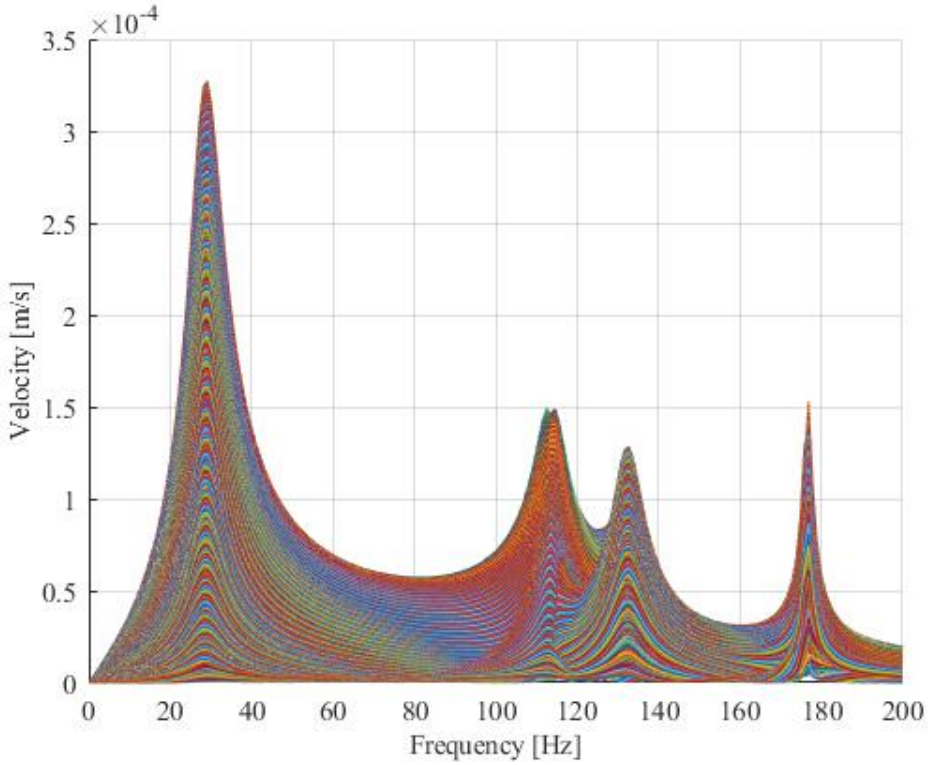

Figure 34. Frequency response function when the model is exposed to a pressure load of 1 Pa, using the modified damping. The response is plotted for all 14681 nodes of the surface.

The damping can obviously be modified until an exact match is found. This was however not done, since running these analyzes are very time consuming with large amounts of data to handle due to the velocity extraction from 14681 nodes. Getting an exact match would not server any specific purpose other than giving an opportunity to evaluate the damping, and this purpose is considered to be fulfilled with the modified damping. The calculated sound pressure level L_p with modified damping is shown in table 11 and the difference relative to the measured sound pressure level is visualized in figure 35.

Table 11. Measured and predicted sound pressure level using the modified damping according to table 10.

Frequency (Hz)	29	114	132	177
L_p measured (dB)	38.474	72.613	76.377	81.129
L_p modified damping (dB)	38.201	73.285	76.157	81.272

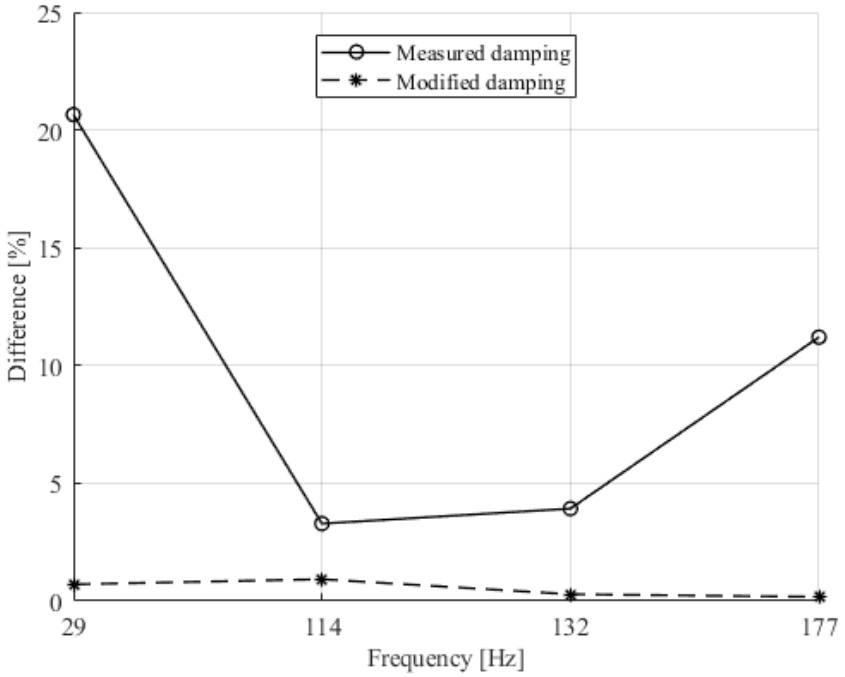

Figure 35. The difference between measured and predicted sound pressure levels using the measured damping and modified damping.

Once the sound pressure level is calculated in the receiving room, the sound reduction index $R_w(f)$ is calculated with the use of equation 3.5. If the sound pressure level obtained from the model matches with the measured results, the sound reduction index will obviously match as well. The reverberation time measurements started from 50 Hz due to lower frequency recordings being unavailable with the equipment used. Therefore, the sound reduction index at the first resonance mode (29 Hz) was calculated with the absorption area determined at 50 Hz. The predicted sound reduction index, using the modified damping in the model, together with the measured is displayed in table 12.

Table 12. Measured and predicted sound reduction index using the modified damping according to table 10.

Frequency (Hz)	29	144	132	177
Measured R_w (dB)	20.47	26.96	26.13	25.09
Predicted R_w (dB)	20.11	26.08	26.14	25.14

8 Discussion

When first starting this project, a three-layer CLT was analyzed with multiple EMA measurements to determine its properties. Due to different circumstances a five-layer CLT slab was later used during the transmission measurements. The 5-layer CLT is a different structure with different parameters and in order to determine these, data from an identical EMA study on a 5-layer CLT floor was acquired from measurements made by Cheng Qian [32]. This data was then analyzed in order to determine resonance frequencies and modal shapes.

When performing the EMA measurements on the three-layer CLT it became clear that the boundary conditions had a huge impact on the results. The floor in the lab room was not completely flat and the steel beams were placed at different locations in order to find a surface where they would have a stable standing point. It was however not possible to find a position where there was no gap somewhere between the floor and the beam and even if the gap only was a few millimeters, the movement of the beams could be felt by simply walking on them. When analyzing the data from these measurements the FRF showed unclear acceleration peaks that seemed to be dampened out which meant that it was hard to identify the resonance frequencies. This gave questionable mode shapes that can be seen in appendix C. When running the MAC comparison, which also can be found in appendix C, it was clear that the mode shapes from the measurements and the Abaqus model were not matching in an acceptable manner.

The EMA measurements for the five-layer CLT slab gave better results because of better boundary conditions, where the beams stood on a flatter surface. Other factors could have affected the measurements such as the fact that the clamps connecting the CLT to the beams (figure 11) might not have been equally tightened. The steel beams were not attached to the floor in any way which means that horizontal movement could have occurred, with only friction between the beams and the floor being the restraining force. Bad hits with the modal hammer was also registered but those would just have a minor impact on the results, if any at all, since an average of three hits on each point was used.

Different boundary conditions were tested in the Abaqus model in order to get as close as possible to the actual boundary conditions being used for the EMA measurements. An example of this was having the boundary conditions set as lines along the slab compared to having them set as surfaces resembling the contact area between the CLT and the beams. The difference between the two was very small and barely had any impact at all. The rigidness did however have a major impact on the results where more rigid boundaries resulted in higher eigenfrequencies for each mode. First, fully restrained conditions were tested on both sides in the model but gave eigenfrequencies that were very high compared to those from the measurements. Releasing the restraint in the x-direction on one side gave more realistic results, resembling the measurements the most.

Three rigid body modes appeared in the Abaqus model created in chapter 7, although the slab had been restrained to move at some points to prevent this behavior (figure 29). These modes did however not affect the result since they were damped out. They would not have any impact on the results anyway since the sound pressure radiated from the CLT slab only depends on the velocity in the vertical direction. The rigid body modes could have been avoided by placing the boundary condition in the middle of the depth of the plate instead of at its outer edge.

As shortly discussed earlier, the Abaqus model gave more eigenmodes than the ones found from the measurements and there are several reasons to why this occurred. Some modes might simply not have been excited during the measurements and other modes might have been too complex for the grid that was used, not being able to capture the behavior. Any shear or rigid body modes that were found in the model could also have occurred during the measurements, but the accelerometers only measured the accelerations in the vertical direction which means that no shear modes would show in the post processing.

The Norsonic140 sonometer that was used for the measurements of the reverberation time records in T_{20} or T_{30} and then extrapolates the values to T_{60} assuming linear behavior. During these measurements, the receiving room had a lot of floor insulation and other materials laying around the room which might make this assumption invalid. If this was the case, the error regarding the reverberation time would affect the calculated absorption area and even further the sound reduction index. This brings some uncertainties when it comes to the results of this thesis since the results from the Abaqus model is compared and calibrated with the results from the measurements.

The accelerations were not measured on the actual CLT slab during the transmission measurements which means that no direct comparison could be made with the accelerations from the model. Some information could be lost when the velocities of the plate in the model are converted into sound pressure with Kurzweils approximated relationship (equation 3.13), why a comparison between the accelerations would have been more accurate. It is however doubtful that the accelerometers would accurately capture such low accelerations.

The sound pressure level measurements were, as explained in chapter 7.1, made at different locations in the rooms in arm-height but not close to the CLT slab itself. Both the sending- and retrieving room are during normal conditions reverberant rooms, which means that a diffuse sound field can be assumed and that the sound pressure level should be equal in every point of the room volume. The receiving room did however, as stated earlier in this chapter, have a lot of materials laying around and could no longer be considered a completely reverberant room. This means that the sound pressure level at the surface of the CLT slab, where the sound pressure level from the Abaqus model were calculated, might differ a bit from the measured sound pressure level.

The CLT slab in the step sound laboratory room did, as explained in chapter 7.1, consist of two individual five-layer CLT slabs that were connected in the middle. If this connection was not completely tight some leakage may have occurred and would in that case affect the sound pressure level in the receiving room. It is hard to create a very rigid connection, and it does affect the acoustic vibratory response of the CLT slab. This was not accounted for in the Abaqus model, where it was modelled as one homogeneous plate.

Exposing the model to a pressure load only excited four modes, visible as the four resonance peaks at approximately 29, 114, 132 and 177 Hz. Velocity peaks can only be extracted where peaks are present, leading to an estimation of sound pressure at only 4 frequencies. By this method, the possibility to approximate a sound pressure level in the receiving room at any given frequency is therefore not possible. When the model is run with the measured damping, the resulting sound pressure level is a bit off, as was shown in table 9. However, damping is as previously stated a very elusive parameter. The non-linear characteristics of damping makes it

hard to predict and is not the same in different cases of loading, i.e. a pressure field of small magnitude and the impact of a hammer, due to its amplitude dependent nature.

The modified damping (table 10) which gave the closest resemblance to the measured sound pressure exhibits no consistency, where the damping in some modes where increased and in other decreased with varying magnitude. The damping in the first mode was altered the most and increased from 5% to 15% which is arguably an unreasonably high value. The first mode did however display the largest relative frequency difference in chapter 6.2.2, indicating that this mode was not captured accurately, which might lead to further complications down the road and thus affecting the value of the damping. The modified damping in mode 14 and 15 also deviated largely from the measured damping. These modes are in frequencies above the highest excited resonance frequency at 177 Hz and thus have small, if any, effect on the results. An argument can be made that any arbitrary damping could be set in these two modes.

The method presented in this thesis to predict sound insulation of CLT could still be useful by simply avoiding the damping. If a schematic, standardized damping is applied, different types of CLT can be compared in relation to each other. The in-situ response would likely not be predictable without having full knowledge of the damping, which cannot be known without performing measurements on the CLT once it is mounted in the structure. With a data base containing measured values of sound transmission in CLT buildings, this method could indicate how the sound insulation changes with different CLT slabs and what level of sound insulation that can be expected.

9 Conclusion

The purpose of this thesis was to create an accurate FE model to predict the airborne sound insulation of a CLT slab in the low-frequency range where some conclusions have been drawn along the way. Constructing a FE model to analyze the vibroacoustic response of a CLT slab is permeated with uncertainties. This starts when defining the material parameters. Getting the interaction between the rigidness of the boundary conditions and the stiffness of material parameters right is not an easy task. The parameters are calibrated in relation to the results of the EMA, making these measurements highly impactful on the vibroacoustic response. Uncertainties in the material parameters leads to uncertainties in the boundary conditions, which subsequently brings uncertainties to any result obtained from the model. Making an accurate model to predict the modal shapes and natural frequencies of a CLT slab is, although with a cumbersome parameter calibration, perfectly achievable. However, when it comes to the response in terms of velocities and accelerations, damping has a very large impact on the results. It directly controls the magnitude of the amplitude peaks, making the parameter calibration futile if the damping is unknown.

However, if a correct model is created and the damping is known, it is possible to obtain a velocity response. The velocity level can then be converted into a sound pressure level, that further determines the sound reduction index. In this thesis the conversion between velocities and sound pressure level was made by using Kurzweil approximation, which with some tweaking of the damping yielded accurate results. The problem with the method presented is that the sound pressure level only can be calculated at the resonance frequencies excited by a pressure load. To determine a single value of the sound reduction index R_w according to the current ISO regulations, the sound reduction index $R_w(f)$ needs to be determined for every 1/3 octave band frequency between 50-3150 Hz. It is therefore not possible to determine a single value sound reduction index according to ISO standards by this method. The method can be used in a broader frequency spectrum, but the issue with ISO compatibility would remain. The method does fulfill the goal of predicting the sound insulation in the lower frequencies, although not in 1/3 octave bands.

A suggested solution to the uncertainties of damping is to use a schematic damping when creating FEM models to predict sound transmission, giving the possibility to compare different CLT solutions to one another rather than trying to predict the actual in-situ response. Recommended further research on this topic would be to by this method predict the sound transmission of different CLT slabs with a schematic damping, and then compare it to measured results to investigate if the results from the FEM models are proportional to the measurements.

References

[1] Södra, (2019). *Södras satsning på KL-trä mot nya höjder*. [online] Available at: https://www.sodra.com/sv/travaror/byggsystem-i-tra/Om-kl-tra/ [Accessed 17 Feb. 2019]

[2] Larsson, M., Erlandsson, M., Malmqvist, T. and Kellner, J. *Byggandets klimatpåverkan*. (2016). Stockholm: Svenska Miljöinstitutet.

[3] Hagberg, K. (2018). *Management of acoustics in lightweight structures*. PhD. Lund University.

[4] Sundström, K-H. (2017). *Trä är framtiden*. [online] Available at: https://www.skogsindustrierna.se/siteassets/dokument/presentationer/virkesforum-2017/karl-henrik-sundstrom-stora-enso.pdf [Accessed 13 Feb. 2019]

[5] Svenskt Trä, (2019). *Skogen och hållbart skogsbruk*. [online] Available at: https://www.svenskttra.se/om-tra/att-valja-tra/tra-och-miljo/skogen-och-hallbart-skogsbruk/ [Accessed 15 Feb. 2019]

[6] World Health Organisation. (2018). *Environmental noise guidelines for the European region*. [pdf] Copenhagen: WHO Regional Office for Europe. Available at: http://www.euro.who.int/__data/assets/pdf_file/0008/383921/noise-guidelines-eng.pdf [Accessed 21 Feb. 2019]

[7] Persson, K. (2000). *Micromechanical modelling of wood and fibre material*. PhD. Lund University.

[8] Svenskt Trä, (2017). *Träets styrka och styvhet*. [online] Available at: https://www.traguiden.se/om-tra/materialet-tra/traets-egenskaper-och-kvalitet/mekaniska-egenskaper1/traets-styrka-och-styvhet/?fbclid=IwAR0_G8_N_VEQqp6ZhFSnDGJfdX3SSru0yTN9tJ4TsSWGwDChJgdL4mT2qvg [Accessed 3 Mar. 2019]

[9] Svenskt Trä, (2013). *Att välja trä*. [pdf] Stockholm: Svenskt Trä. Available at: https://www.svenskttra.se/siteassets/6-om-oss/publikationer/pdfer/att-valja-tra.pdf [Accessed 5 Mar. 2019]

[10] SVENSK STANDARD SS-EN ISO 10140-2:2010. *Acoustics – Laboratory measurement of sound insulation of building elements – Part 2: Measurement of airborne sound insulation.* SIS Förlag AB, Stockholm.

[11] SVENSK STANDARD SS-EN ISO 10140-3:2010. *Acoustics – Laboratory measurement of sound insulation of building elements – Part 3: Measurement of impact sound insulation.* SIS Förlag AB, Stockholm.

[12] Vigran, T. (2008). *Building acoustics*. New York: Taylor & Francis.

[13] Ecophon, (2019). Sound insulation. [online] Available at: https://www.ecophon.com/en/acoustic-solutions/acoustic-knowledge-bank/Basic-Acoustics/What-is-sound-insulation/ [Accessed 7 Mar. 2019]

[14] SVENSK STANDARD SS-EN ISO 3382-2:2008. *Acoustics – Measurement of room acoustic parameters – Part 2: Reverberation time in ordinary rooms*. SIS förlag, Stockholm.

[15] Chopra, A. (2012). *Dynamics of structures*. New Jersey: Pearson Education Inc.

[16] Brüel & Kjaer. (2019). *Piezoelectric Accelerometer Types 4507 and 4508*. [pdf] Available at: https://www.bksv.com/en/products/transducers/vibration/Vibration-transducers/accelerometers/4507-001 [Accessed 23 May 2019]

[17] Brüel & Kjaer. (2019). *Modal sledge hammer, 3 Lb*. [pdf] Available at: https://www.bksv.com/en/products/transducers/vibration/Vibration-transducers/impact-hammers/8208 [Accessed 23 May 2019]

[18] Pulse LabShop. (2018). Denmark: Brüel & Kjaer.

[19] BK Connect. (2018). Denmark: Brüel & Kjaer.

[20] Winter, C. (2018). *Frequency Dependent Modeling for the Prediction of the Sound Transmission in Timber Constructions*. PhD. Technical University of Munich.

[21] Labonotte, N. (2012). *Damping in Timber Structures*. PhD. Norwegian University of Science and Technology.

[22] Kurzweil, L. G. (1979). Ground-borne noise and vibration from underground rail systems. *Journal of Sound and Vibration*, 66(3).

[23] Thornely-Taylor, R. (2016). The relationship between floor vibration from an underground source and sound pressure level in the room. In: *23rd International Congress on Sound & Vibration*. [online] Athens. Available at: http://www.ruperttaylor.com/ICSV23.pdf [Accessed 24 May 2019]

[24] Ottosen, N and Petersson, H. (1992). *Introduction to the Finite Element Method*. Harlow: Pearson Education Limited.

[25] Negreira, J. (2016). *Vibroacoustic Performance of Wooden Buildings*. PhD. Lund University.

[26] Allemang, J and Brown, L. *A correlation coefficient for modal vector analysis*. Prof. Mechanical and Industrial Engineering University of Cincinnati.

[27] Matlab. (2017). USA: The MathWorks.

[28] SkogsSverige, (2018). Södra satsar på höga hus i trä: ”Vi tänker storskaligt”. [online] Available at: https://www.skogssverige.se/nyheter/sodra-satsar-pa-hoga-hus-i-tra-vi-tanker-storskaligt [Accessed 23 Feb. 2019]

[29] SVENSK STANDARD SS-EN ISO 10140-4:2010. *Acoustics – Laboratory measurement of sound insulation of building elements – Part 4: Measurement procedures and requirements.* SIS Förlag AB, Stockholm.

[30] Negreira, J., Sjöström, A. and Bard, D. (2015). Low frequency vibroacoustic investigation of wooden T-junction. *Applied acoustics 105 (2016) 1-12*, [online] Available at: https://www.sciencedirect.com/science/article/pii/S0003682X15003400 [Accessed 15 May 2019].

[31] Lindblad, S. (2019). Akustik. In: *Nationalencyklopedin*. Stockholm: Ne Nationalencyklopedin Ab.

[32] Qian, C. (2019). *Development of a Vibroacoustic Stochastic Finite Element Prediction Tool for a CLT Floor*. Applied Science 9(6)

Appendix

A. Convergence check five-layer CLT (EMA model)

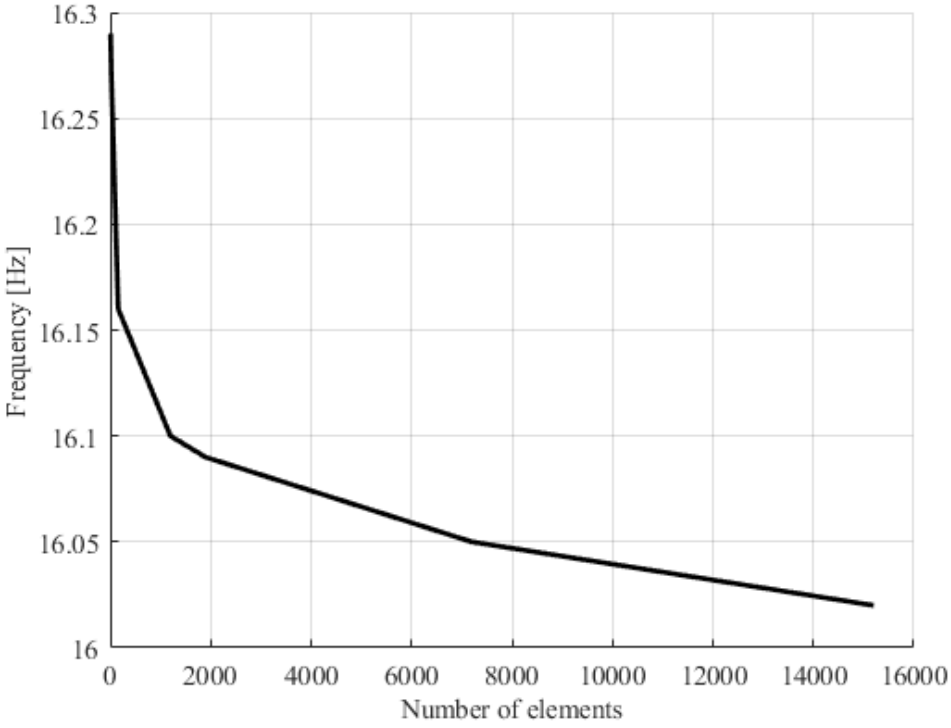

Figure 36. Element size convergence, mode 1.

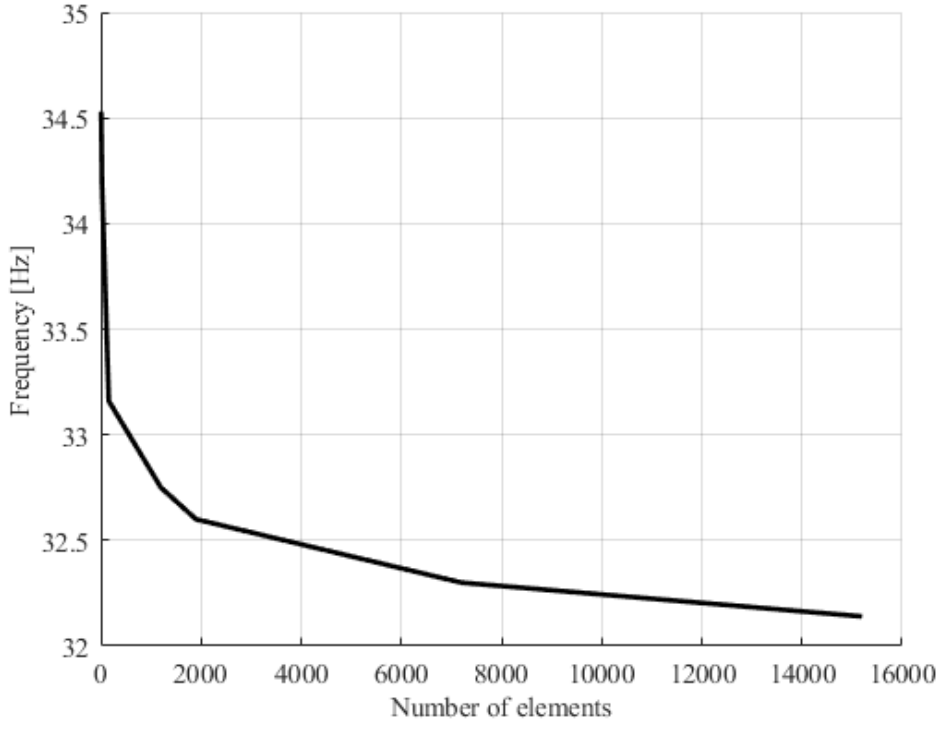

Figure 37. Element size convergence, mode 2.

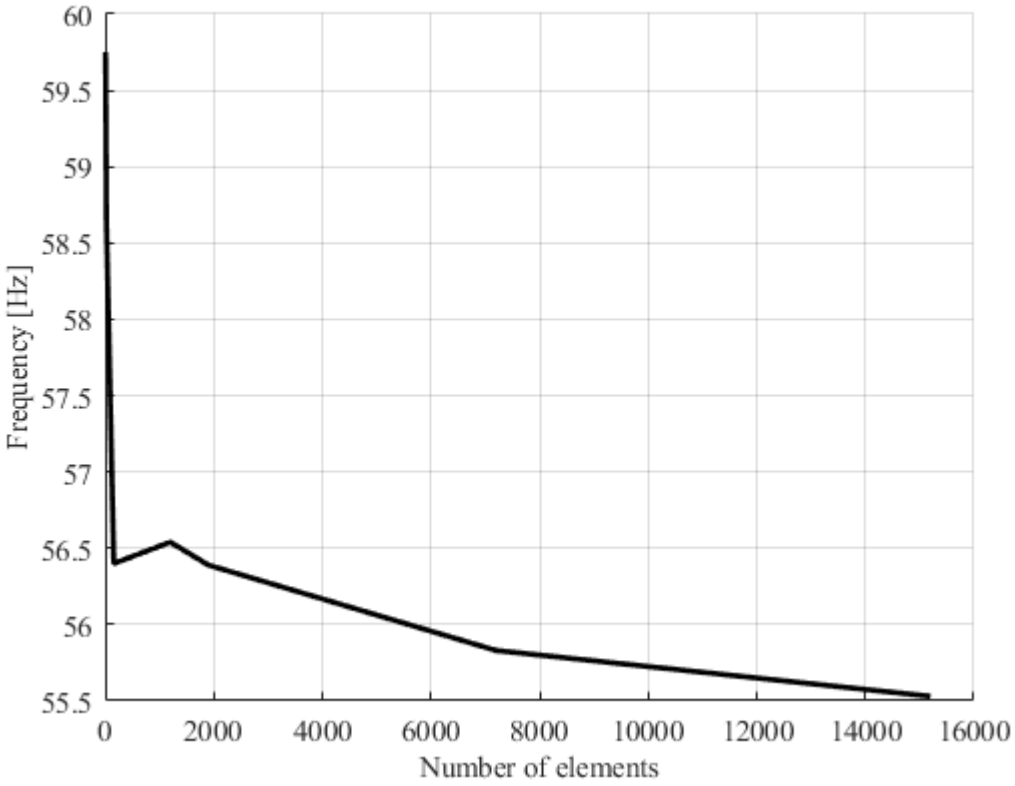

Figure 38. Element size convergence, mode 3.

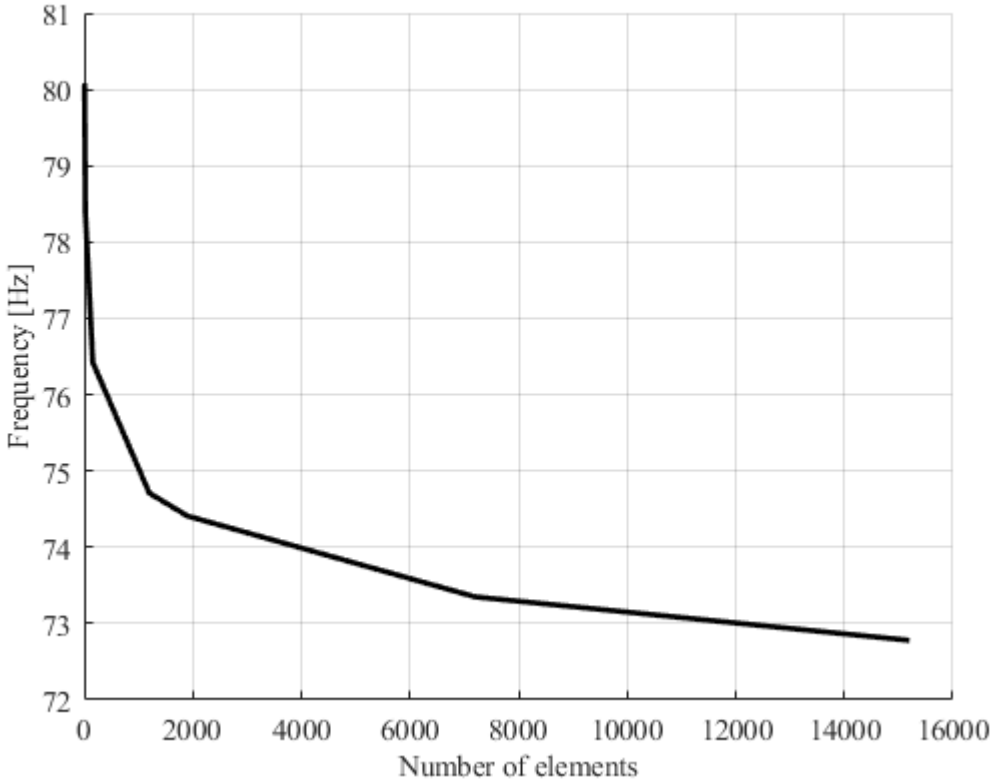

Figure 39. Element size convergence, mode 4.

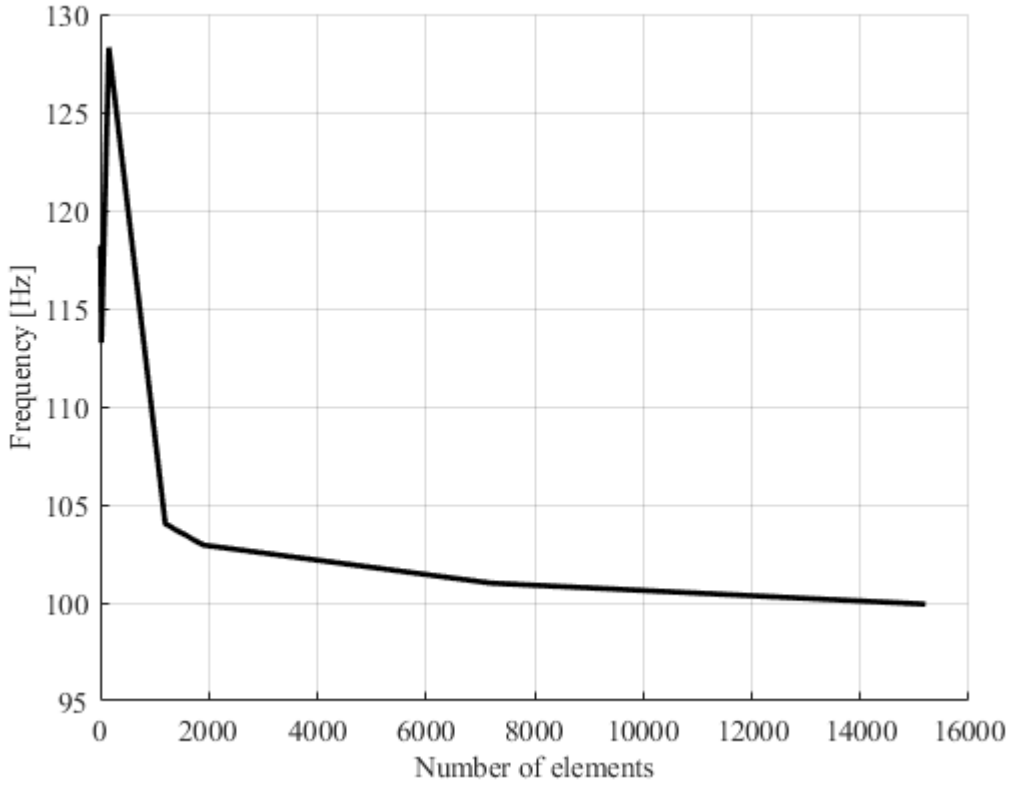

Figure 40. Element size convergence, mode 5.

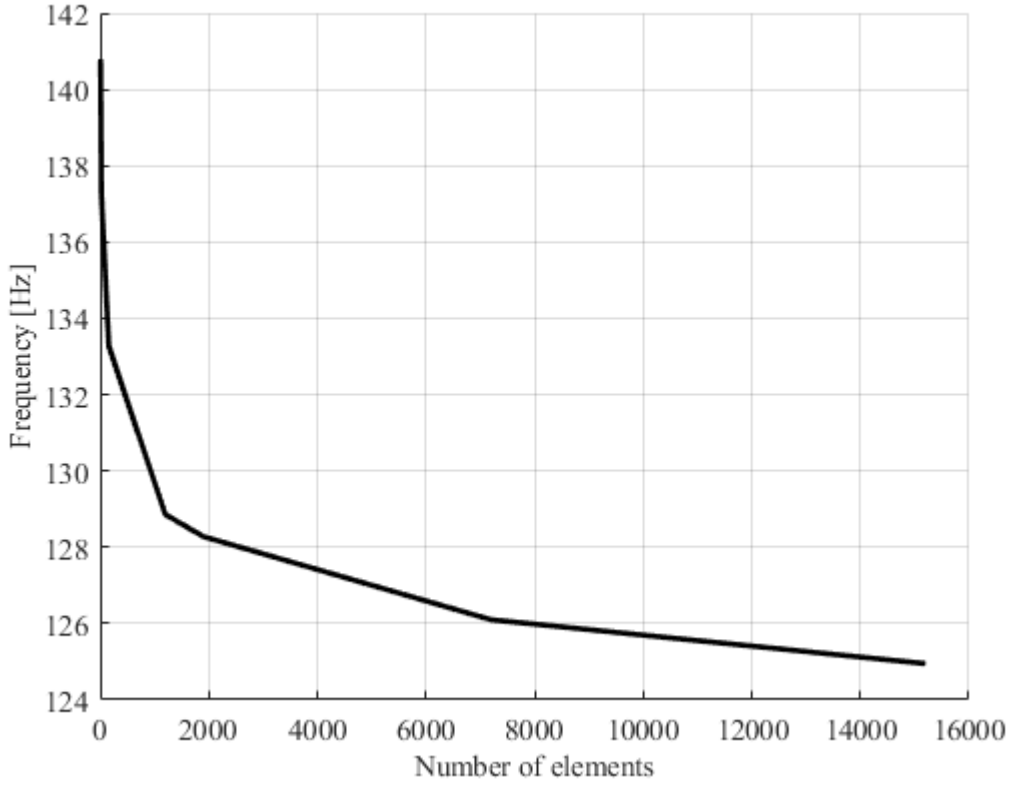

Figure 41. Element size convergence, mode 6.

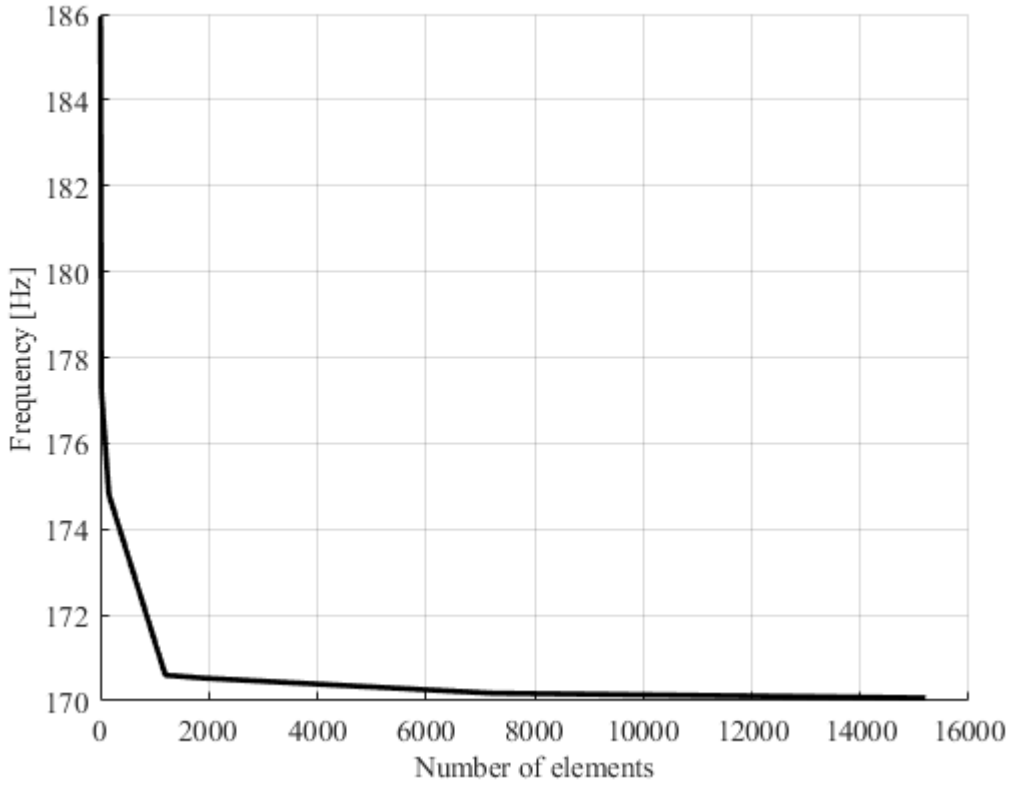

Figure 42. Element size convergence, mode 7.

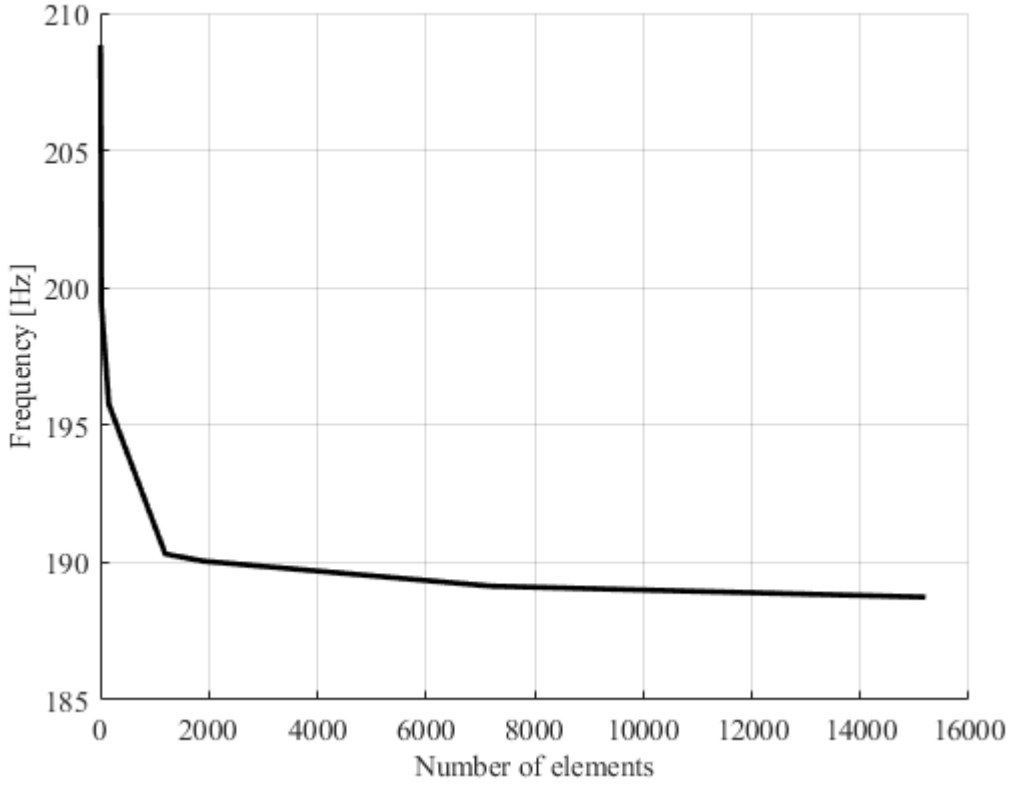

Figure 43. Element size convergence, mode 8.

B. Convergence check five-layer CLT (Sound reduction model)

B.1 Element convergence

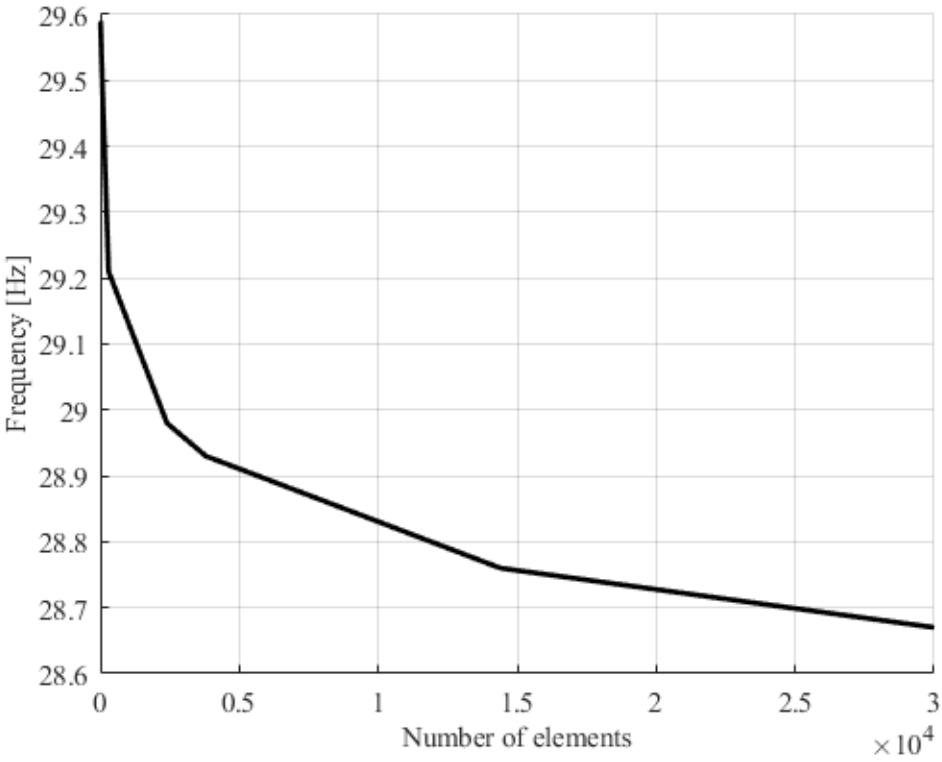

Figure 44. Element size convergence, mode 1.

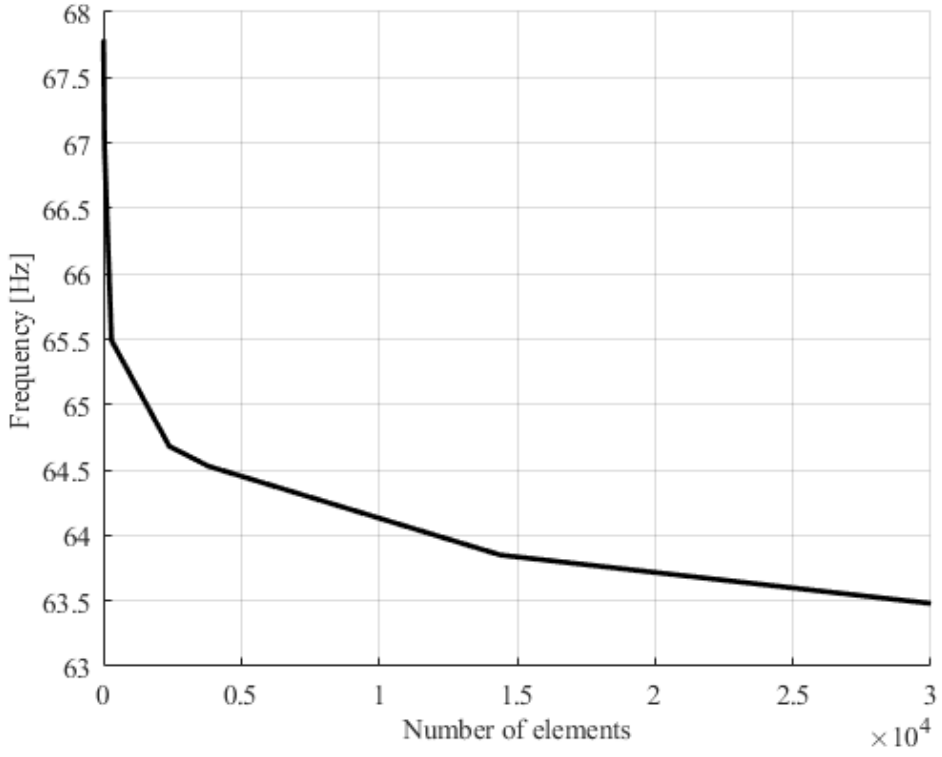

Figure 45. Element size convergence, mode 2.

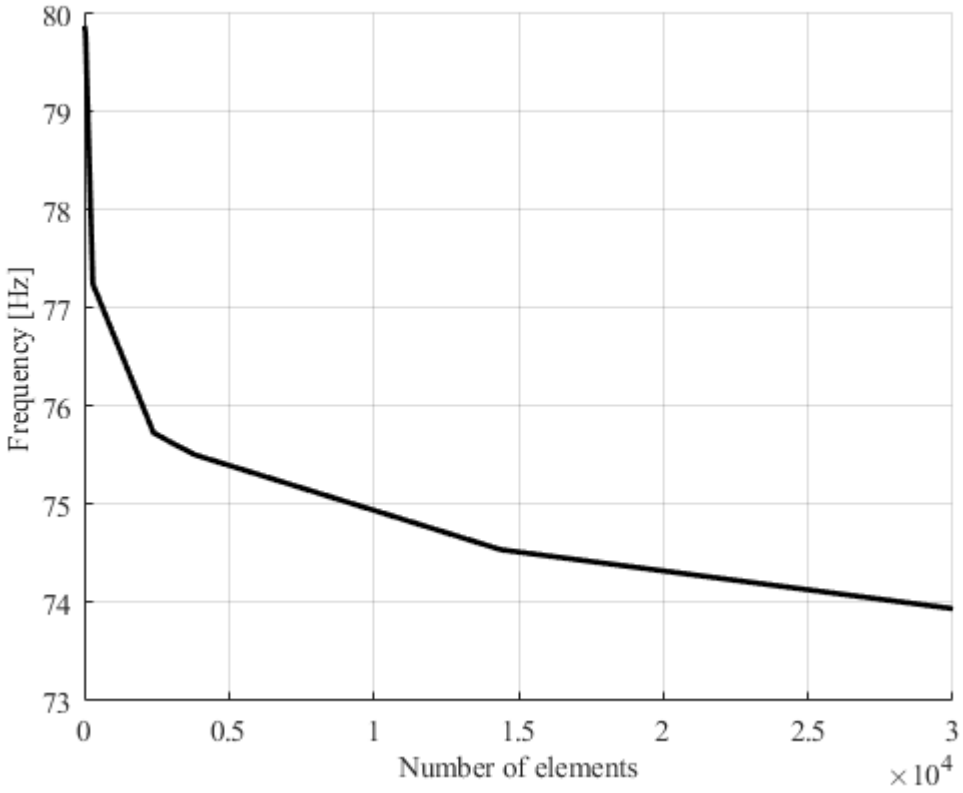

Figure 46. Element size convergence, mode 3.

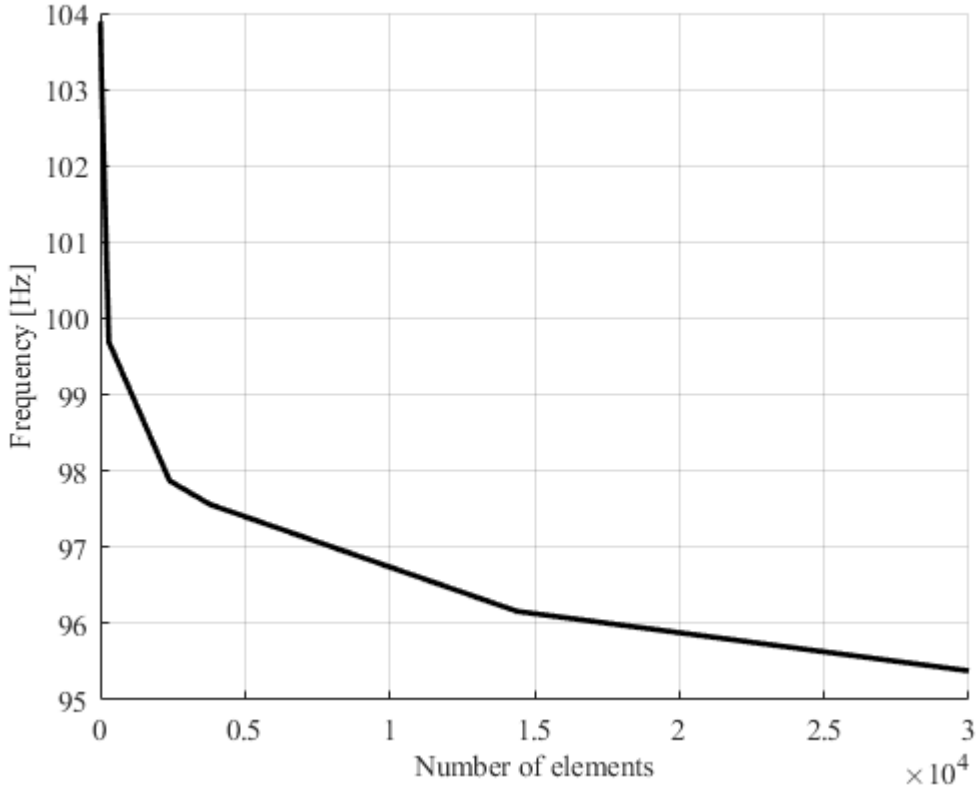

Figure 47.Element size convergence, mode 4.

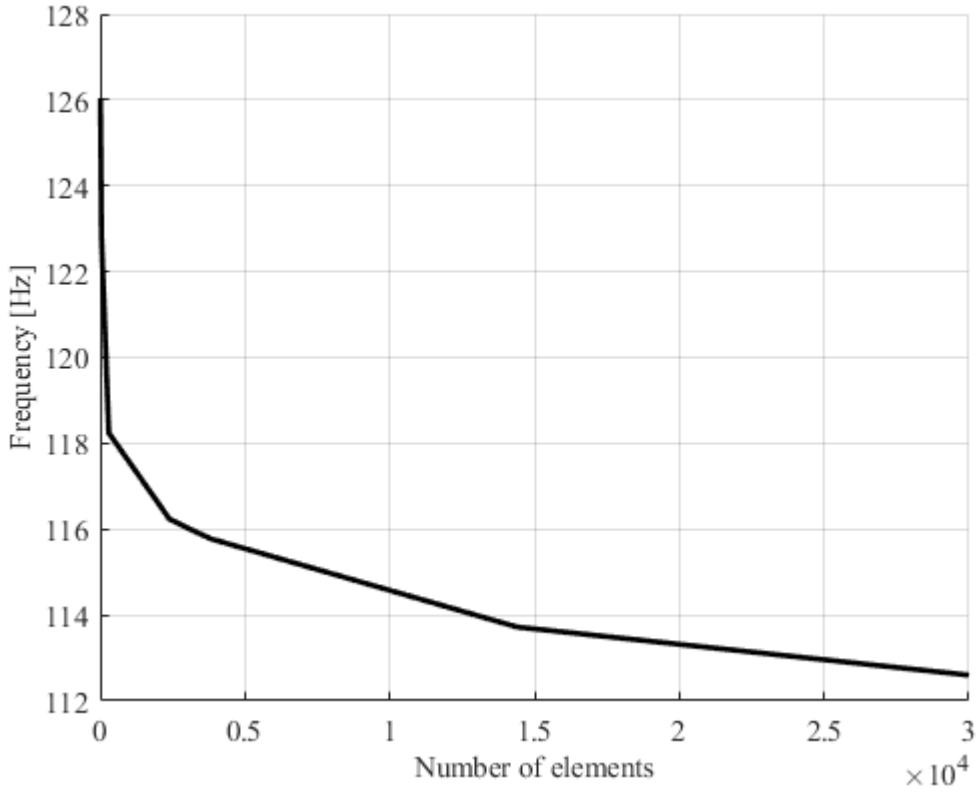

Figure 48. Element size convergence, mode 5.

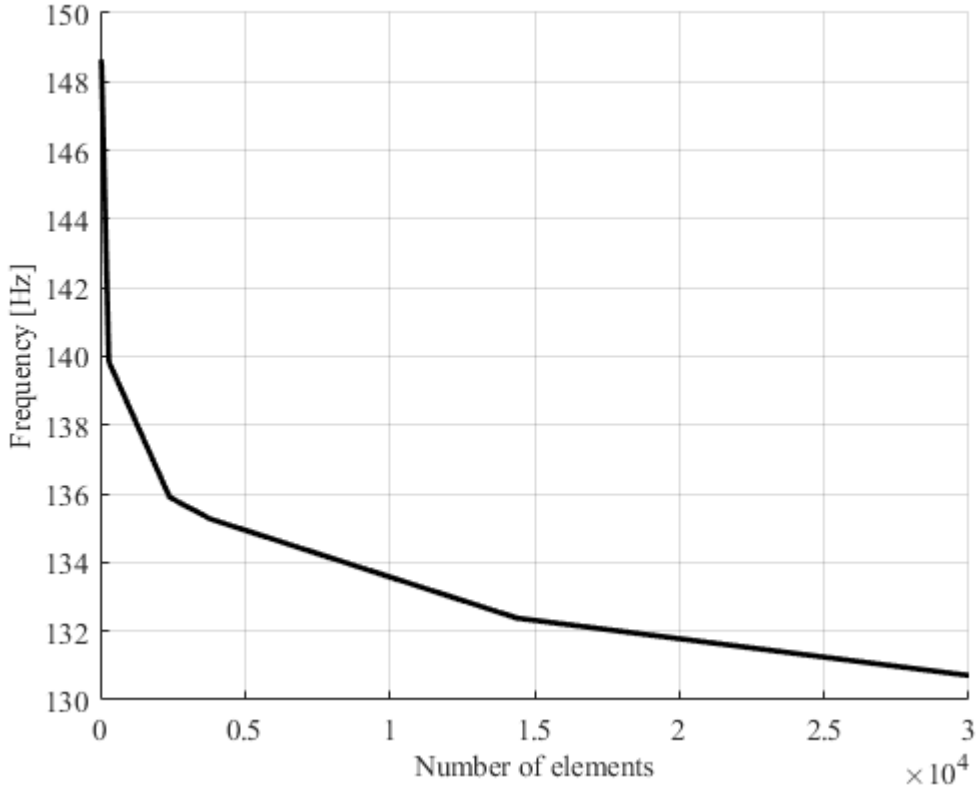

Figure 49. Element size convergence, mode 6.

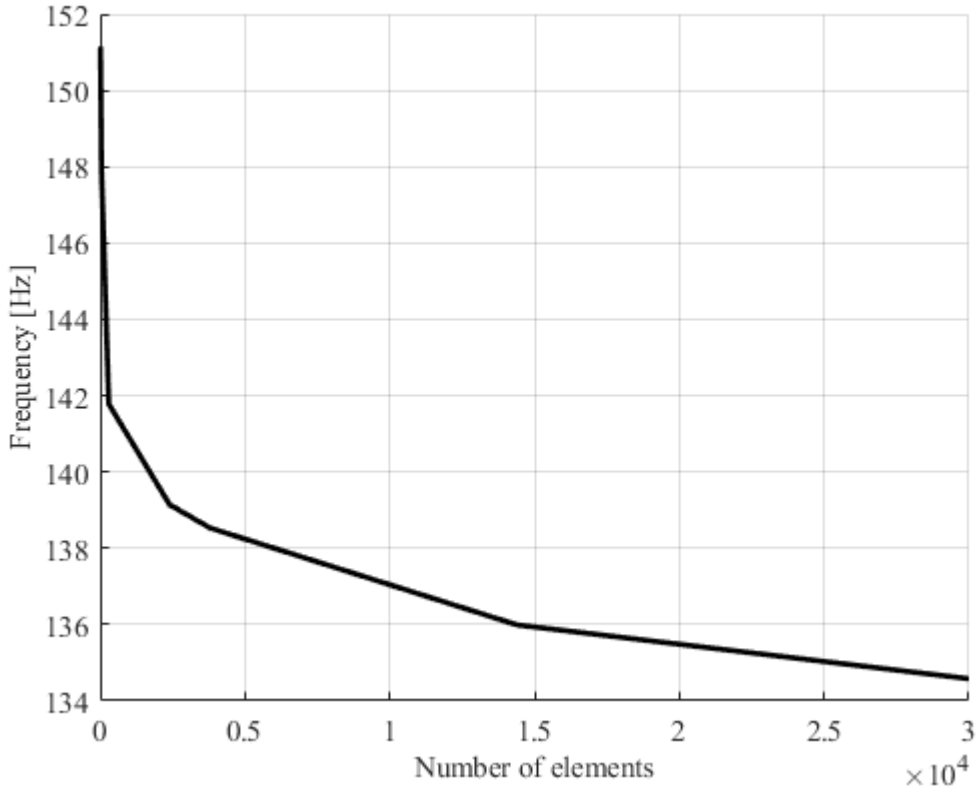

Figure 50. Element size convergence, mode 7.

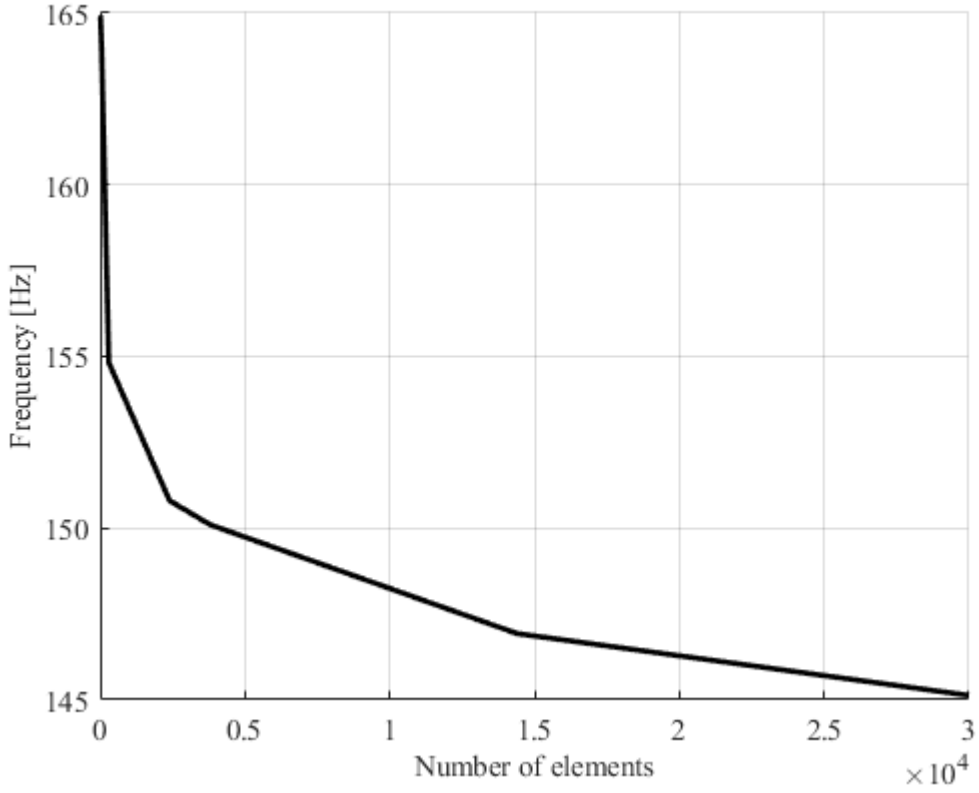

Figure 51. Element size convergence, mode 8.

B.2 Increment convergence

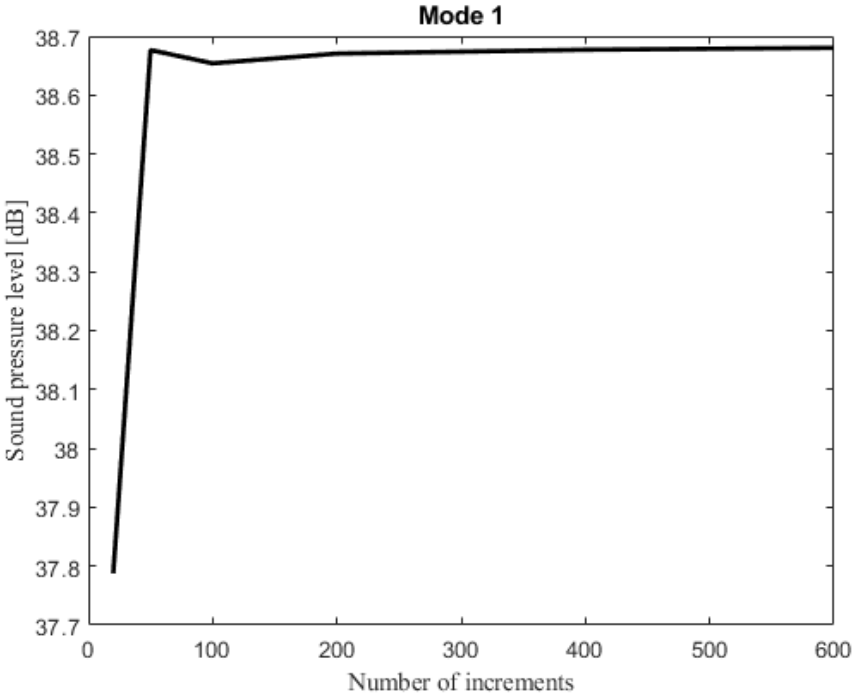

Figure 52. Increment size convergence, resonance mode 1.

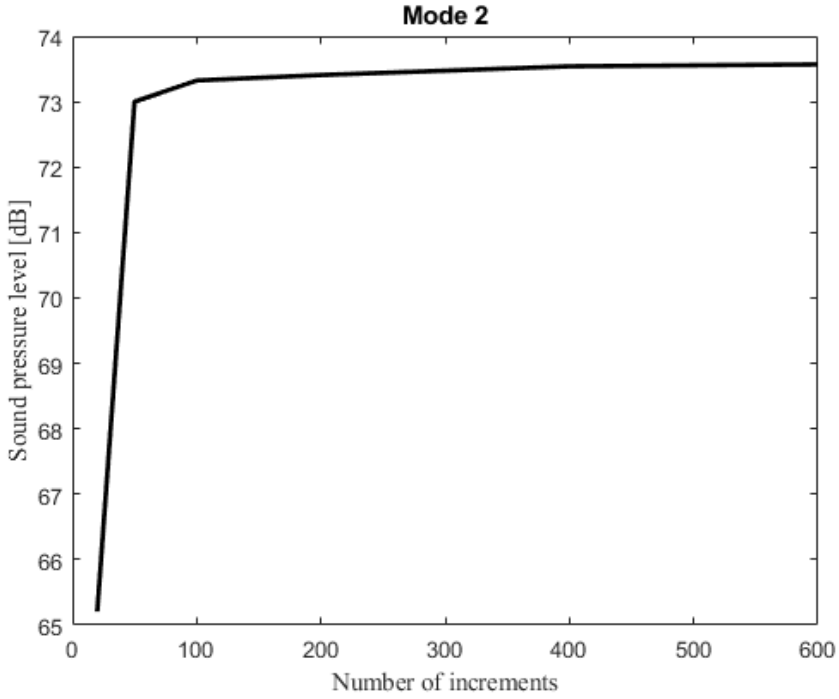

Figure 53. Increment size convergence, resonance mode 2.

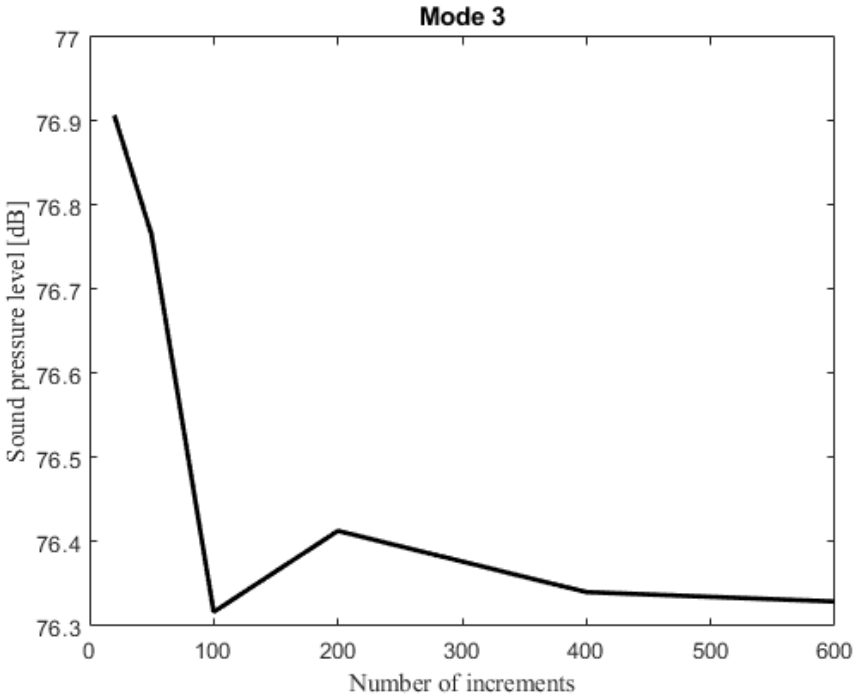

Figure 54. Increment size convergence, resonance mode 3.

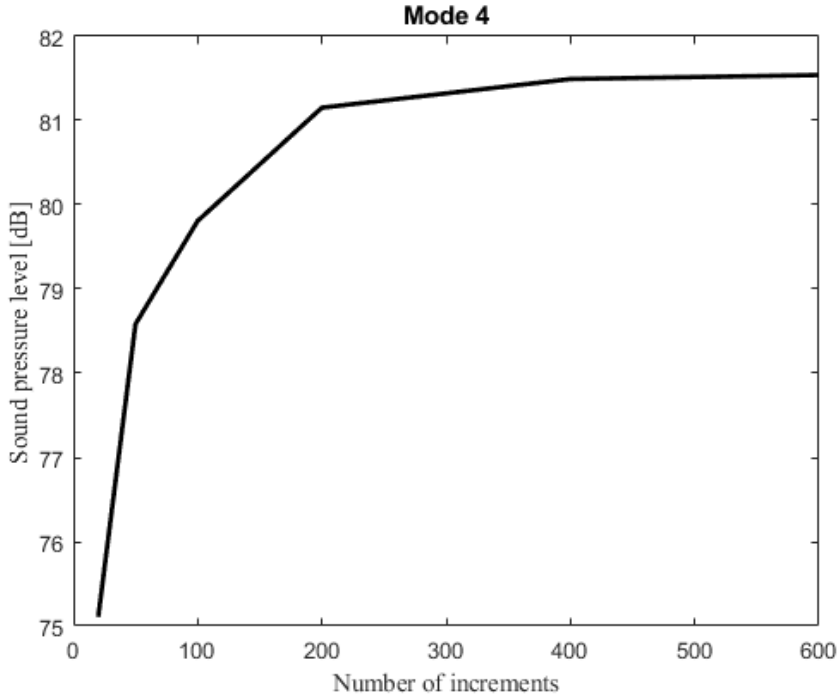

Figure 55. Increment size convergence, resonance mode 4.

C. Measurement results, three-layer CLT

Figure 56. Measurement setup, 3-layer CLT

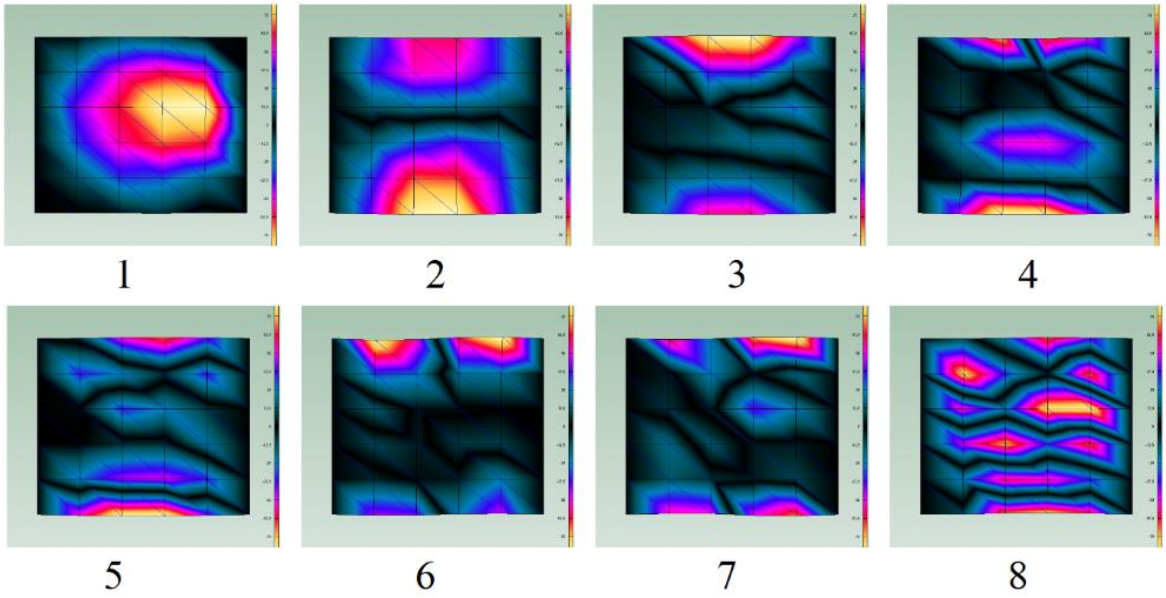

Figure 57. EMA modes, 3-layer CLT

Modes	1	2	3	4	5	6	7	8
1	0,723	0,073	0,327	0,015	0,063	0,005	0,007	0,006
2	0,014	0,887	0,056	0,318	0,006	0,005	0,024	0,048
3	0,068	0,008	0,785	0,041	0,25	0,003	0,026	0,063
4	0,004	0,088	0,022	0,822	0,045	0,009	0,007	0,064
5	0,03	0,012	0,229	0,005	0,802	0,006	0,0034	0,0073
6	0,001	0,003	0,002	0,002	0,001	0,628	0,004	0,042
7	0,009	0,002	0,011	0	0,012	0,048	0,442	0,037
8	0,001	0,127	0,011	0,26	0,009	0,012	0,062	0,558

Figure 58. MAC values, 3-layer CLT